Silent Crickets Reveal the Genomic Footprint of Recent Adaptive Trait Loss

Sonia Pascoal[1†], Judith E. Risse[2,3†], Xiao Zhang[4†], Mark Blaxter[5,6], Timothee Cezard[5], Richard J. Challis[5], Karim Gharbi[5,7], John Hunt[8,9], Sujai Kumar[5], Emma Langan[5,10], Xuan Liu[11], Jack G. Rayner[4], Michael G. Ritchie[4], Basten L. Snoek[12,13], Urmi Trivedi[5], Nathan W. Bailey[4*]

[1]Department of Zoology, University of Cambridge, CB2 3EJ, United Kingdom
[2]Bioinformatics, Department of Plant Sciences, Wageningen University & Research, 6708 PB Wageningen, The Netherlands
[3]Animal Ecology, Netherlands Institute of Ecology, PO Box 50, 6700 AB Wageningen, The Netherlands
[4]School of Biology, University of St Andrews, St Andrews, Fife KY16 9TH, United Kingdom
[5]Edinburgh Genomics, University of Edinburgh, Edinburgh EH9 3JT, United Kingdom
[6]Institute of Evolutionary Biology, University of Edinburgh, Edinburgh EH9 3JT, United Kingdom
[7]Earlham Institute, Norwich Research Park, Norwich NR4 7UZ, United Kingdom
[8]School of Science and Health and the Hawkesbury Institute for the Environment, Western Sydney University, Penrith, NSW 2751, Australia
[9]Centre for Ecology and Conservation, University of Exeter, Cornwall Campus, Penryn TR10 9FE, United Kingom
[10]School of Environmental Sciences, University of East Anglia, Norwich Research Park, Norwich NR4 7UZ, United Kingdom
[11]Centre for Genomic Research, University of Liverpool, Liverpool L69 7ZB, United Kingdom
[12]Theoretical Biology and Bioinformatics, Utrecht University, Padualaan 8, 3584 CH Utrecht, The Netherlands
[13]Terrestrial Ecology, Netherlands Institute of Ecology, PO Box 50, 6700 AB Wageningen, The Netherlands

† Contributed equally
* Correspondence: nwb3@st-andrews.ac.uk

Secondary trait loss is widespread and has profound consequences, from generating diversity to driving adaptation. Sexual trait loss is particularly common[1]. Its genomic impact is challenging to reconstruct because most reversals occurred in the distant evolutionary past and must be inferred indirectly[2], and questions remain about the extent of disruption caused by pleiotropy, altered gene expression and loss of homeostasis[3]. We tested the genomic signature of recent sexual signal loss in Hawaiian field crickets, *Teleogryllus oceanicus*. Song loss is controlled by a sex-linked Mendelian locus, *flatwing*, which feminises male wings by erasing sound-producing veins. This variant spread rapidly under pressure from an eavesdropping parasitoid fly. We sequenced, assembled and annotated the *T. oceanicus* genome, produced a high-density linkage map, and localised *flatwing* on the X chromosome. We characterised pleiotropic effects of *flatwing*, including changes in embryonic gene expression and alteration of another sexual signal, chemical pheromones. Song loss is associated with pleiotropy, hitchhiking and genome-wide regulatory disruption which feminises flatwing male pheromones. The footprint of recent adaptive trait loss illustrates R. A. Fisher's influential prediction that variants with large mutational effect sizes can invade genomes during the earliest stages of adaptation to extreme pressures, despite having severely disruptive genomic consequences.

Male crickets sing to attract and court females and to fight with rivals, but approximately 15 years ago, silent *T. oceanicus* males arose and spread in populations on the Hawaiian archipelago[4,5] (Fig. 1a). They were first detected in 2003 in a population on Kauai, where they rapidly spread to near-fixation from undetectable starting frequencies, under selection imposed by a lethal parasitoid fly, *Ormia ochracea* (Fig. 1b)[4]. Female flies acoustically locate male crickets by eavesdropping on their songs, but silent flatwing males have feminised wings lacking structures used to produce sound and are thus protected (Fig. 1c). The genetic mutation(s) underlying the flatwing phenotype show Mendelian segregation and X-linkage[6,7], and the propagation of flatwing males to near-fixation in the Kauai population represents one of the fastest rates of evolution known in the wild, having occurred in fewer than 20 generations[4]. All males found in a comprehensive survey of this population in October 2018 were flatwing (38 flatwing males, no normal-wing males found or heard singing by JGR and NWB), but the continued existence of the population indicates that silent males still find mates and must compensate for their inability to sing. The selective environment promoting

the rapid spread of flatwing crickets is understood, but the mechanistic basis of the phenotype remain an open question. How did such a spectacularly disruptive phenotypic change invade the genome of crickets so quickly? Foundational evolutionary theory predicts that adaptive variants which invade genomes and spread under positive selection should tend to be small in effect size and exert few pleiotropic consequences, although exceptions are predicted during the earliest stages of adaptation[8,9]. Empirical studies have been unable to address this in naturally-evolving systems.

The locus controlling the expression of flatwing morphology could have arisen through *de novo* mutation(s) coinciding with the time of the phenotype's first observation in 2003, it could have invaded the genome of the Kauai population via migration from an unknown location elsewhere in Hawaii (flatwing morphs have not been observed outside of the Hawaiian islands), or it could have existed for much longer in the population but at extremely low levels, evading detection by researchers. Studies of insecticide resistance in insects and of melanic morphs of Lepidoptera provide some precedent. While some museum specimens collected before the invention of organophosphates have been shown to contain insecticide-resistance alleles[10], in other cases, resistance alleles arose *de novo*, and also invaded populations and spread under selection[11]. In the peppered moth, a canonical example of rapid evolution in the wild, melanism had a single recent origin approximately corresponding to the start of the industrial revolution[12,13], but melanic morphs are common in many insects and may persist at low frequencies due to negative pleiotropy, at least until favourable selective conditions occur[14]. In *T. oceanicus*, parasitoid pressure pre-dated the appearance of flatwing in the Kauai population[4], thus the *de novo* or introduction scenarios are most plausible.

We studied the genomic signature of song loss in the population on Kauai where flatwing crickets were first discovered, and in which rapid spread has been most thoroughly documented[4]. We sequenced the *T. oceanicus* genome, generating an assembly of 2.045 Gb consistent with flow cytometry size estimates[7], with a scaffold N50 of 62.6 kb (Extended Data Table 1). We established an F_3 mapping population using crosses designed to maximise recombination on the X chromosome, which is only diploid in females (Extended Data Fig. 1). Mapping offspring and parents were sequenced using RADseq, and a map was assembled containing 19 linkage groups. *T. oceanicus* has a haploid chromosome number of (13+X). We identified linkage group 1 (LG1) as the X chromosome by applying coverage and

heterozygosity filters and dummy coding putative X-markers prior to constructing the map. LG1 was the largest linkage group, with a female recombination length of 379 cM and a male length of 195 cM (Extended Data Fig. 2). After resolving chimeric scaffolds (Extended Data Table 2), 35.6% of the genome was anchored to a linkage map using a LOD5 cutoff (Extended Data Table 3) (Fig. 2a).

We performed gene prediction and annotation using custom pipelines incorporating *ab initio*, homology, and transcriptome-based approaches (Extended Data Fig. 3). Evidence from different gene prediction and annotation methods was weighted and filtered to predict a final, conservative set of 19,157 genes, 75% of which had functional annotation (Extended Data Table 4, Extended Data Fig. 4). Gene density was assessed (Fig. 2a track i), and we tested whether the putative X linkage group showed a different distribution of repeat content relative to the other linkage groups, across eight common categories of repeats. It did not (Fig. 2a track iii, Extended Data Table 5, Extended Data Fig. 5). *T. oceanicus* gene features were compared to 10 other insect species (Extended Data Table 6), and we contrasted transposable element classifications with three other recently published insect genomes (Extended Data Table 7). The *T. oceanicus* genome and metadata associated with it are curated in ChirpBase (www.chirpbase.org), a GenomeHubs Ensembl genome browser[15] that we created as an openly available, community-based genomics resource for researchers working on singing insects.

Flatwing was definitively mapped to the putative X chromosome (Fig. 2b) using markers supported by a LOD10 cutoff and a mixed model, ANOVA-based approach designed to control for uneven genomic relatedness caused by family structure in the mapping crosses. To cope with the particularly high marker association on the putative X chromosome caused by the Mendelian mode of inheritance of *flatwing* and the different effective population size of the X compared to autosomes, we identified the QTL using only the top 1% of markers after FDR correction, yielding a prominent peak occupying approximately one third of the X chromosome (Fig. 2c). Flatwing morphology is observable in males during mid- to late-instar stages of juvenile development, so we examined early embryonic gene expression differences associated with *flatwing*. Females carrying the genotype cannot be visually distinguished and embryos cannot be readily sexed, so we used replicate laboratory lines homozygous for *flatwing* or *normal-wing* genotypes to detect widespread differential gene expression in the

developing thoraces of embryonic crickets. We found 830 genes differentially expressed (DE), 204 of which had a $\log_2$ fold-change > 1, and a predominant pattern of down-regulation in *flatwing* crickets (Extended Data Table 8, Extended Data Fig. 6). DE genes associated with *flatwing* were widely distributed across linkage groups and unmapped scaffolds (Fig. 2a track iv).

These physically dispersed expression effects suggest that *flatwing* acts as a master regulatory switch during early development, with a broad cascade of downstream effects. Pathways reconstructed using differential expression data are consistent with such a mode of action. For example adherin junction activity was enriched, which affects epithelial patterning during early development (Extended Data Tables 9 & 10). Using a stringent and redundant approach combining information from gene sets identified in the QTL study, RNA-seq experiment and a previously-published bulked segregant analysis[7], we identified 51 annotated protein-coding genes located within LG1 as top flatwing-associated candidates (Extended Data Table 11). GO enrichment analysis indicated that *positive regulation of developmental process* was overrepresented in this candidate gene set, with three genes in particular (*NBL1, GOGA4, UNC89*) known to play a fundamental role in the regulation of cell differentiation (Extended Data Table 12).

In most pterygote insects, wings are derived from imaginal discs formed during development by the invagination of embryonic ectoderm[16]. Previous work mainly in *Drosophila melanogaster* has established that the developmental elaboration of wing venation patterns requires the involvement of numerous transcription factors and complex coordination across numerous signalling pathways[17]. Here, we found that 8 of 51 flatwing associated candidate genes have reported involvement in *D. melanogaster* wing development. For example, *stat92E* expands the proximodistal axis of the wing imaginal disc, subdividing and patterning it[18]. *Collier* encodes a transcription factor required for wing disc patterning[19], and *Myoglianin* expression is required for normal wing disc development[20]. *ROR1* encodes a transmembrane tyrosine-protein kinase receptor involved in phosphorylating MAP kinases[21], and reduction of MAPK activity through *ROR1* silencing can lead to a loss of wing venation phenotype[17]. The protein krasavietz is encoded by *PKRA*, and establishes planar cell polarity in the wing[22], disruption of which can lead to wing distortion[23]. Knockouts and mutants in *Pelle*, *Gen5*, and *Plexin-A4* show wing shape and venation alterations with features similar to flatwing[24-26].

We tested the consequences of the rapid invasion of *flatwing* into the *T. oceanicus* genome by focusing on a distinct, close-range sexual signalling modality that operates alongside acoustic signalling in field crickets. Cuticular hydrocarbons (CHCs) are long-chain, waxy molecules expressed on insect cuticles. CHCs are thought to have evolved for dessication resistance, and they tend to be expressed as a bouquet of numerous individual hydrocarbon compounds. *T. oceanicus* CHCs are sexually dimorphic and function as sexual signals during male and female mate choice[27-29], and they have been found to vary between flatwing and normal-wing male crickets[30]. We characterised the CHC profiles of F_3 mapping individuals, all of which were raised in a common garden environment, by extracting their CHCs and using gas chromatography – mass spectrometry (GCMS) to measure the abundance of 26 individual compounds (Fig. 3a) (Extended Data Table 13). By performing dimension reduction using principal components (PC) analysis of the CHC profiles, we first established that, in our mapping population, males carrying *flatwing* showed noticeable and significantly different CHC profiles from *normal-wing* males (Fig. 3b) (multivariate analysis of variance on 6 principal components with eigenvalues > 1 describing male CHC blends: $F_{6,191} = 29.769$, $p < 0.001$) (Extended Data Table 14).

QTL analysis was then performed on the first six CHC PCs to determine whether *flatwing*-associated variation in male CHC profiles mapped to identifiable genomic regions. The putative X chromosome, LG1, was of particular interest, because we hypothesized that the striking variation between CHC profiles of flatwing and normal-wing males could be a pleiotropic effect of *flatwing*. Genetic mapping of CHCs was performed blind to male morphotype. PC1, which explained over a third of the variance in male CHC profiles, mapped to a ca. 2.5 cM region strongly co-localised with *flatwing* (Fig. 3c). PCs 4 and 6 also had co-localizing peaks (Extended Data Fig. 7). As dimension reduction for CHCs can obscure phenotypic patterns in the original individual chemical compounds, we mapped each of the 26 compounds separately. Of these, 9 showed significant peaks co-localising with *flatwing* (Fig. 3d). We recovered no autosomal QTL peaks for PCs 1-6, and only one QTL peak for one compound on one autosome (compound 11, 7-C31ene, on LG8). However, the latter peak was weakly supported, with only a single marker showing an association at FDR-corrected $p < 0.001$.

We interrogated genes on scaffolds under the CHC QTL peaks following a similar procedure used to produce the *flatwing* candidate gene set (Extended Data Table 15). Of 55 protein-coding genes, a subset of 6 were implicated for every CHC trait with a significant QTL peak, and these 6 genes were also present in the *flatwing* candidate gene set. These are strong candidates for testing the pleiotropic consequence of evolved acoustic sexual signal loss on chemical sexual signals. Our final step was to explore the nature of the phenotypic shift in flatwing male CHC profiles. It is unknown how flatwing males' profiles compare to those of females[30], but given the generally feminising effect of *flatwing* on male wing morphology, we predicted that flatwing males' CHC profiles would also be feminised. We compared them to the profiles of normal-wing males and females using discriminant function analysis on profiles from all three groups. Discriminant function 1 (eigenvalue = 2.526) explained 78.8 % of the variance, and indicated that flatwing male crickets' CHC profiles are strongly feminised (Fig. 3e). Their CHCs appear to be correspondingly less attractive to females[31].

The rapid emergence and spread of flatwing crickets on Kauai has been described as one of the fastest rates of evolutionary adaptation ever documented in the wild[32]. Nearly a century ago in 1930, R. A. Fisher[8] developed a 'geometric' model that describes the genomic landscape of such early-stage adaptation and predicts what mutational features are associated with adaptive change. In doing so, he reconciled the prevailing, gradualist view of evolution with seemingly inconsistent units of discrete Mendelian inheritance that were being discovered and characterised at the time. Fisher's key insight was that the process of evolutionary adaptation tends to favour mutations of small effect, with impacts narrowly limited to the phenotypic variants directly under selection[33]. However, he built exceptions to this general rule into his model when selection is severe, and the genomic signature of song loss in Hawaiian *T. oceanicus* uniquely confirms and illustrates this insight. Adaptation was recent, abrupt and proceeded rapidly in this system. Prior work on *T. oceanicus* has found differences in the level of phenotypic plasticity, gene expression, and other reproductive characteristics such as male testis size between male *normal-wing* and *flatwing* genotypes[34-36], and our present findings reveal the genomic footprint of strong, associated effects on sexual signalling in an entirely different sensory channel. These consequences of rapid adaptive trait loss are early-acting, genome-wide, and impact a range of important fitness traits. The suite of characters affected in flatwing crickets is reminiscent of feminised alternative male morphs in ruff (*Calidris pugnax*) in which supergene architecture controls

size, ornament and behavioural traits simultaneously[37], and in feminised bulb mites[38]. What is surprising is that an evolved loss of function could lead to such similarly wide-ranging phenotypic impacts so quickly. The genomic signature of recent, rapid trait loss in *T. oceanicus* confirms Fisher's predictions about adaptive evolution – by demonstrating the exception to his rule.

METHODS

Cricket rearing and maintenance. Laboratory stocks of *Teleogryllus oceanicus* were established from eggs laid by wild-caught females from a population on the Hawaiian island of Kauai in 2012, and a population near Daintree, Australia in 2011. Stocks were maintained in the laboratory within 16 L plastic containers containing cardboard egg cartons for shelter. All crickets were reared in a single, temperature-controlled chamber a 25 °C, on a 12:12 light:dark cycle. They were maintained regularly and fed *ad libitum* with Burgess Excel Junior and Dwarf rabbit pellets and provided water in a moist cotton pad that also served as an oviposition substrate. Throughout all experiments, all crickets were reared in a common-garden environment in the same temperature-controlled chamber.

Genome sequencing. Three Illumina sequencing libraries were prepared using genomic DNA extracted from the head capsule and muscle tissue of a single *T. oceanicus* female using a DNeasy Blood & Tissue kit (Qiagen). The female was sourced from the Kauai stock population. gDNA was quality-checked using Nanodrop and Qubit prior to Illumina library preparation and sequencing at Edinburgh Genomics. We prepared three standard paired-end TruSeq libraries with insert sizes of 180 bp, 300 bp, and 600 bp. We supplemented reads from the above three Illumina libraries with additional sequences from two TruSeq Nano Pippin selected libraries with insert sizes of 350 bp and 550 bp, one 8 kb Nextera gel-plus mate-pair library, and 1 PacBio library. For these libraries, gDNA from a separate, single female cricket from the same laboratory population was extracted using a high molecular weight Genera Puregene Cell Kit (Qiagen). The first three TruSeq libraries were sequenced on 5 lanes of an Illumina HiSeq 2000 v3 to yield 100 bp paired-end reads. NanoPippin libraries and the Nextera mate-pair library were sequenced on 2 Illumina HiSeq 2500 lanes to yield 250 bp paired-end reads. To construct the PacBio library, we purified the extraction with 1x AMPure beads (Agencourt) and performed quality control using Nanodrop and Qubit. Average DNA size and degradation was assessed using a high sensitivity genomic kit on a fragment analyzer. Size-selected and non-size-selected libraries were made by shearing gDNA using g-TUBEs (Covaris). Size selection was performed using the BluePippin DNA Size Selection System with 0.75% cassettes and cutoffs between 7 and 20 kb. Preparation of both libraries then proceeded using the same protocol. We treated DNA for 15 min at 37 °C with Exonuclease V11. DNA ends were repaired by incubating

for 20 min at 37 °C with Pacific Biosciences damage repair mix. Samples were then incubated with end repair mix for 5 min at 25 °C followed by washing with 0.5x AMPure and 70% ethanol. DNA adapters were ligated overnight at 25 °C. Incubation at 65 °C for 10 min was used to terminate ligation reactions, and then samples were treated with exonuclease for 1 hr at 37 °C. We purified the SMRTbell library using 0.5x AMPure beads and checked quality and quantity using Qubit assays. Average fragment size was quantified using a fragment analyser. For sequencing, primers were annealed to the SMRTbell library at values determined using PacBio's Binding Calculator. A complex was formed using DNA polymerase (P6/C4 chemistry), bound to MagBeads, and then used to set up 43 SMRT cells for sequencing to achieve 10X coverage. Sequencing was performed using 240 min movie times.

Genome assembly. Raw reads from all Illumina libraries were trimmed using cutadapt v.1.8.3[39] to remove adapters, primers and poor quality bases, and then error-corrected using BLESS[40]. PacBio reads <1,000 bp were discarded. The original fragment length of the 350 bp library was shorter than the sequenced paired read length of 500bp, so reads from this library were merged using Vsearch v.1.10.1[41]. Platanus v.1.2.4[42] was used to assemble error-corrected reads from all Illumina libraries except the mate-pair library; reads from the latter were added at the scaffolding stage. Next, we selected the contigs >1,000 bp and combined these with the PacBio data to generate a hybrid assembly using PBJelly v.15.2.20[43]. Pilon v.2.1[44] was used to improve local base accuracy, and BUSCO v.2.1[45] was used to assess genome quality through gene completeness.

Repeat annotation. We used *de novo* and homology-based approaches to identify repetitive regions. We first built a *de novo* repeat library using RepeatModeler[46], with dependencies RECON and RepeatScout[47]. To scan and classify interspersed repeats and low complexity DNA sequences at the DNA level, we searched the cricket genome sequence against the Dfam consensus database[48], RepBase[49], and the *de novo* repeat library using RMBlast[50] and RepeatMasker[51]. Protein-level repeats were identified by searching against the TE Protein Database using RepeatProteinMask[51]. Unclassified repetitive elements were further classified by TEclass[52], a programme using a support vector machine learning algorithm. Tandem repeats were also identified in the cricket genome using Tandem Repeat Finder[53].

Gene prediction. Before running gene prediction pipelines, repetitive regions identified above were masked using an in-house Perl script. We built a pipeline including *ab initio*, homology and transcriptome-based methods to predict protein-coding genes in the cricket genome (Extended Data Fig. 3). For *ab initio* prediction, SNAP[54], Glimmer-HMM[55], GENEID[56], and BRAKER1[57] were used to generate preliminary gene sets from the repeat-masked genome. Specifically, reads obtained from the *T. oceanicus* transcriptome were aligned against the repeat masked genome with TopHat2[58]. SAMTOOLS[59] was used to sort and index the resulting Binary Alignment Map (BAM) format file.

This BAM file was processed in BRAKER1[57], which used transcriptome data to train GENEMARK-ET[60], generate initial gene structures, and then subsequently train AUGUSTUS[61] and finally integrate RNA-seq information into final gene predictions. For other *ab initio* gene prediction programmes, gene sets from *Locusta migratoria*[62], *Acyrthosipon pisum*[63], and *Drosophila melanogaster*[64] were used for model training. For homology-based prediction, we aligned protein sequences of five insect species (*L. migratoria*[62], *Drosophila melanogaster, Anoplophora glabripennis*[65], *Nilaparvata lugens*[66], and *Cimex lectularius*[67]) to the repeat-masked cricket genome using TBLASTN ($E < 10^{-5}$)[50]. The boundaries of potential genes were further identified using BLAST2GENE[68]. We then ran GENEWISE2[69] to obtain accurate spliced alignments and generate a final, homology-based gene set. For prediction based on transcriptome data, the *de novo* transcriptome assembly generated by Trinity[70] was filtered based on gene expression level, and then passed to Program to Assemble Spliced Alignments (PASA)[71]. PASA performed transcript alignments to the cricket genome, generated a new transcript assembly, and predicted gene structures. All gene sets predicted by *ab initio*, homology, and transcriptome-based methods were then combined into a weighted consensus gene set using EVidenceModeler (EVM)[72]. We removed genes likely to be spurious, those with low EVM support, partial genes with coding lengths shorter than 150 bp, and genes only supported by a minority (≤ 2) of *ab initio* methods[73]. PASA was used to further update the filtered consensus gene set to produce a finalised official gene set. The completeness of this final gene set was assessed by both BUSCO v.2.1 (using the arthropoda dataset)[45] and transcriptome data.

Functional assignment. Putative gene functions were assigned based on InterPro[74], SwissProt[75], TrEMBL[75] and RefSeq non-redundant (NR) protein and Kyoto Encyclopedia of Genes and Genomes (KEGG) gene databases. Briefly, we first obtained protein sequences from the final gene set using EVM[72]. Functional annotation and gene ontology terms were assigned to genes based on protein sequence, using InterProScan 5[76]. These proteins were also blasted against SwissProt, TrEMBL and NR databases (PLASTP, $E < 10^{-5}$), and assigned their best hits as functional annotations. Gene ontology (GO) terms were assigned using GO annotations downloaded from the GO Consortium[77,78]. BLAST2GO[79] was implemented to further assign unassigned genes using NCBI databases, and KEGG Orthology (KO) terms were assigned using BlastKOALA[80].

Genome anchoring. ALLMAPS[81] was used to detect chimeric scaffolds, anchor the cricket genome to the linkage map (see below), and construct pseudo-molecules (reconstructed portions of chromosomal sequence). We first built a consensus genetic map based on male and female genetic distances obtained from linkage maps, in which equal weighting was applied for both sexes. Then, scaffolds for which more than four markers mapped to multiple linkage groups were designated as chimeric scaffolds, and split. After this correction was applied, scaffolds anchored to the linkage maps were oriented and ordered based on the consensus genetic map. We used a custom Perl script to order

unanchored scaffolds according to their length, and liftOver[82] to convert genome coordinates based on anchoring results.

Genome browser development (ChirpBase). We created ChirpBase, an open-access community genomics resource for singing insects, such as field crickets and katydids. The resource can be accessed at www.chirpbase.org where users may view and download genomic data and scripts presented in this study in addition to uploading data. An index page links to an ensembl page, where assembly statistics can be visualised using a Challis plot or compared in tabular format. A plot illustrating codon usage is presented, as well as a visualisation of BUSCO scores. Additional pages linking from this include a basic local alignment search tool (BLAST) page and a download page where raw data can be accessed. We used the GenomeHubs framework to set up ChirpBase[14]. Briefly, the databased is hosted using a Linux container (LXC) on a remote computer, linked to a cluster via an intermediate import computer. A MySQL docker container was started in the LXC, where a database *ini* file resided to guide additions to the database. An Ensembl-easy mirror Docker container was run to import the database into the MySQL container, uploading data designated in the *ini* file from the LXC to the database. The MySQL container links to an Ensembl EasyMirror container, BLAST container, and a download container.

Linkage and QTL mapping crosses. We constructed a linkage map for *T. oceanicus* using a series of crosses to maximise recombination on the X chromosome (Extended Data Fig. 1), combined with restriction-site associated DNA sequencing (RAD-seq) to identify markers. *Flatwing* segregates on the X chromosome in both Kauai and Oahu populations[6,7], so mapping was performed with F_3 offspring to increase recombination on the X. We set up two parental mapping families by crossing a flatwing sire from the Kauai population with a virgin dam from the Daintree, Australia population. Daintree females were used in the cross because flatwings do not exist in that population, and other sexually-selected traits such as song and cuticular hydrocarbons show significant divergence between Australian and Hawaiian populations[83], which maximised our opportunity to genetically map segregating variation in other phenotypes. Female F_1 offspring from parental crosses were heterozygous for *flatwing*, enabling recombination on the X. Full-sib matings were then performed with F_1 males, all of which were normal-wing. The resulting F_2 female offspring were a segregating mix of homozygous *normal-wing* genotypes on the X, or heterozygous with respect to wing morph. Recombination between *flatwing* and *normal-wing* genotypes was similarly possible in the heterozygous F_2 females, but their phenotype is not externally detectable. To further increase recombination on the X, we performed another generation of crossing by mating F_2 females with full-sib *flatwing* males from the same generation. Screening male morph types in the resulting F_3 offspring enabled us to identify F_2 crosses involving heterozygous females, as all male offspring of homozygous *normal-wing* females expressed normal-wing morphology. The crossing procedure

resulted in 10 F_3 mapping families from the original two parental families, for a total of 192 females, 113 normal-wing males, and 86 flatwing males.

Marker identification using RAD-seq. RAD-seq was used to identify single nucleotide polymorphisms (SNPs) in F_3 offspring (n = 391), P_0 dams and sires (n = 4), and the F_2 sires and dams (n = 19) that were used to produce mapping individuals in the F_3 generation. For each individual, gDNA extraction and quality control was performed as described above prior to library preparation. gDNA was digested using SbfI (New England BioLabs). We barcoded individuals by ligating P1 adapters (8 nM), then sheared and size selected 300-700 bp fragments. After ligating P2 adapters to sheared ends, parents were sequenced to an average coverage of 120x and offspring to 30x on an Illumina HiSeq 2000.

Construction of linkage map. Reads from all paired end RAD libraries were demultiplexed by sample using process_radtags from Stacks[84], mapped against the reference genome assembly using BWA-MEM[85] and duplicates marked using PicardTools MarkDuplicates (http://broadinstitute.github.io/picard). Variants were called using samtools mpileup (version 1.3, parameters -d 2000 -t DP,DPR,DV,DP4,SP -Aef -gu) and bcftools call (version 1.3, parameters -vmO z -f GQ). The resulting variants were filtered using vcfutils.pl (included with bcftools) with minimum quality 50 and a minimum read depth of 150 (-Q 50 -d 150) to only retain high quality variants. The vcf format was converted to the required lepmap2 input format using a custom script of the RADmapper pipeline (RAD_vcf_to_lepmap_with_sexmarker_conversion.py, https://github.com/EdinburghGenomics/RADmapper). During this conversion samples that did not fit relatedness expectations and samples from family J (which lacked a genotyped father) and P0 parents were excluded from linkage map creation. Putative X-linked markers (male_het <=1, female_het > 20, het_sire <=1) were converted to biallelic markers in the relevant male offspring and sires using a dummy allele (Extended Data Table 17). The linkage map was then created using the following steps and parameters in lepmap2 (Filtering: dataTolerance 0.05 keepAlleles=1; SeparateChromosomes: losLimit=10 sizeLimit=10 informativeMask=3;JoinSingles: lodLimit=5;OrderMarkers: filterWindow=10 polishWindow=100; OrderMarkers evaluateOrder: filterWindow=10 polishWindow=100). The resulting linkage map files were merged with the marker and sample information using a custom script from the RADmapper pipeline (LG_to_marker.py).

QTL mapping. To identify the flatwing locus on the putative X chromosome (LG1), we performed ANOVA for each marker using the lm package in R (v. 3.1). Individual p-values were corrected to account for multiple testing using Bonferroni correction and markers supported by a LOD10 cutoff were plotted. QTL for all 26 cuticular hydrocarbon (CHC) peaks as well as the principle components from the CHC analysis were mapped to the linkage groups using mixed linear models in ASReml 4. Mapping used a GWAS-type approach, taking into account genetic relatedness between individuals[86].

The markers mapped to the autosomal linkage groups 2-19 were filtered to contain only bi-allelic SNP markers with a MAF <=0.01 and <5% missing samples per marker. In addition, all grandparental, parental and female samples were removed together with samples that clustered with the wrong family or did not have CHC data. Only male samples were selected, as our aim was to map male CHCs (not sex-related associations) on the putative X (LG1) and autosomes using principle components from the CHC analysis as well as individual compounds as traits. The remaining 21,047 markers were used to calculate pairwise genetic relatedness with the first normalisation[87]. The resulting inverse relatedness matrix was used as random effect in a model: CHC trait ~ mu marker r! Giv(animal). P-values for all markers were extracted from the results and corrected for multiple testing using Bonferroni correction. The same model was used to assess LG1 separately with the same set of samples, for which 6,537 markers were used after filtering.

Pure-breeding lines and embryo sampling for RNA-seq. Lines homozygous for the *flatwing* and *normal-wing* genotypes were produced following previously described methods[34]. Briefly, one generation of crosses was performed, starting with the laboratory population derived from Kauai and crossing males of either wing phenotype to virgin females of unknown genotype. Because the phenotypic effects of *flatwing* are sex-limited, family-level screening of the resulting male offspring was performed to select homozygous *flatwing* and homozygous *normal-wing* lines, resulting in a final selection of three pure-breeding lines for each morph genotype. Developing embryos were sampled from eggs laid by females from each line. Females were maintained in laboratory culture as above, and their oviposition substrates were monitored. Eggs were removed from the substrate and immediately preserved in 500 µL of RNAlater (Qiagen) at the stage when eye pigmentation first develops, ca. 2 weeks after laying. This time point corresponds approximately to embryonic stage 13-14 in the related grylline species *Gryllus bimaculatus*[88]. After removing the outer egg chorion, the thoracic segment of each nymph was microdissected. Nymphs cannot be sexed based on external morphology until a later stage of juvenile development, and as chromosomal sex determination is XX/XO, screening for sex-specific markers is not possible. To minimise potential variation in sex ratio of samples between lines, and ensure a sufficient volume of tissue to extract RNA, thoracic tissue from n = 8 nymphs was pooled for each replicate, and 6 biological replicates were produced for each morph type (2 per line).

RNA-seq and gene expression profiling. Total RNA was extracted using the TRIzol plus RNA purification kit (Life Technologies) and DNAse treated using PureLink (Invitrogen). RNA was quantified and quality checked using Qubit assessment (Invitrogen) and Bioanalyser RNA Nano Chips (Agilent), respectively. To isolate mRNA we depleted samples with RiboZero. After verifying depletion, cDNA libraries were constructed using the ScriptSeq protocol (Epicentre) with AMPure XP beads for purification. Following barcoding and multiplexing, final quality was checked and qPCR performed using Illumina's Library Quantification Kit (Kapa). Sequencing was performed on an

Illumina HiSeq 2000 v3, with 1% PhiX DNA spike-in controls to produce 100 base paired-end reads. CASAVA v.1.8.2 was used to demultiplex reads and produce raw fastq files, which were then processed with Cutadapt v.1.2.1[38] and Sickle v.1.200[89] to remove adaptor sequences and trim low-quality bases. Further quality assessment was performed in FastQC. Expression analysis of RNA-seq data was performed broadly following the protocol published by Pertea et al. (2016)[90]. Reads were aligned to the genome using HISAT2 with strand-specific settings, and transcripts compiled for each sample in StringTie, using the gene annotation file as a reference, which were then merged across all samples to produce a single annotated reference transcriptome. Sample transcript abundances were estimated with the parameter -e specified to restrict abundance estimation to annotated transcripts. Differential expression analysis was performed at the gene level following normalisation of counts by trimmed mean of M-values (TMM), using a generalised linear model (GLM) with negative binomial distribution and a single predictor variable of 'morph' in the edgeR package[91] in R v.3.4.1. Only genes with an expression level greater than 1 count per million in at least 3 samples were included in the analysis. Significance-testing was performed using likelihood ratio tests, and genes were considered significantly differentially expressed between morph genotypes if FDR-adjusted P-values were below a threshold of 0.05.

Screening for top candidate genes associated with flatwing. We adjusted *P*-values for significant marker associations in the flatwing QTL mapping procedure using Bonferroni correction with a cut-off of $P < 0.001$. Three sources of information were used to comprehensively and robustly detect a set of top candidate genes associated with the flatwing phenotype. We detected genes (i.e. any overlapping portion of a predicted gene sequence cf. Extended Data Table 6) located in 1 kb flanking regions of all significant QTL markers after FDR correction as above, and defined these as QTL-associated candidates. We then subsetted these genes to retain only those located in the 1 kb flanking regions of the most significant (top 1%) of all QTL markers, and defined these as Top 1%-associated candidates. We also obtained the flatwing-associated sequences from a previously published bulk segregant analysis (BSA) of Kauai flatwings[7], and defined the BSA reference sequences containing flatwing-associated SNPs as flatwing-associated BSA sequences. We mapped these BSA sequences to the *T. oceanicus* reference genome using BWA-MEM with default parameters[85]. Coordinates of mapped sequences were extracted from the resulting BAM files using SAMTOOLS[59] and custom Perl scripts, and we only retained those sequences that were anchored to LG1. Genes within 1 kb of these retained sequences were defined as BSA-associated candidates. Finally, we extracted differentially expressed genes from the embryonic thoracic transcriptome analysis above, and defined these as DEG-associated candidates. To ensure a reliable final candidate gene set for flatwing, we only retained genes supported by at least two of these four gene sets. We used KEGG pathway mapping (colour pathway) to reconstruct pathways and obtain reference pathway IDs[92]. To characterise significantly enriched GO terms and KEGG pathways in DEGs, we implemented the hypergeometric

test in enrichment analyses. *P* values for each GO and KEGG map term were calculated and FDR-adjusted in R.

Cuticular hydrocarbon extraction and gas chromatography-mass spectrometry. We extracted CHCs from F_3 mapping individuals prior to extracting gDNA for RADseq. Extraction and analysis of CHCs followed previous methodology[83], which is briefly described here. Subjects were flash-frozen for several minutes at -20 °C and then thawed. They were individually placed into 4 mL borosilicate glass vials (QMX Laboratories) and immersed for 5 minutes in 4 mL of HPLC-grade hexane (Fisher Scientific), then removed from the vials and stored for later processing. We evaporated a 100 µL aliquot of each sample overnight in a 300 µL autosampler vial (Fisher Scientific). CHC extracts were transported to the University of Exeter for gas chromatography mass spectrometry (GC/MS) using an Agilent 7890 GC linked to an Agilent 5975B MS. Extracts were reconstituted in 100 µL of hexane with a 10 ppm pentadecane internal standard, and 2 µL of this was injected into the GC/MS using a CTC PAL autosampler at 5 °C. The carrier gas was helium and we used DB-WAX columns with a 30 m x 0.25 mm internal diameter and 0.25 µm film. Injection was performed in split-less mode. The column profile was optimised for separation of the CHC extract[83] to start at 50 °C for 1 minute, followed by a temperature ramp of 20 °C per minute until finally holding at 250 °C for a total run time of 90 minutes. The inlet temperature was 250 °C and the MS transfer line was 230 °C. We recorded electron-impact mass spectra using a 70 eV ionization voltage at 230 °C, and a C_7-C_{40} alkane standard was run as a standard to enable the later calculation of peak retention indices.

Quantification and analysis of CHC profiles. For each individual, we used MSD CHEMSTATION software (v.E.02.00.493) to integrate the area under each of 26 CHC peaks (Extended Data Table 13) following Pascoal et al. (2016)[83]. Peak abundances were standardized using the internal pentadecane standard and $\log_{10}$ transformed prior to analysis. After accounting for samples that failed during extraction or during the GC run (n = 9), plus one normal-wing male CHC profile that was identified as an outlier and removed during analysis (Extended Data Fig. 8), we analyzed a total of n = 86 flatwing males, n = 112 normal-wing males, and n = 185 females of unknown genotype. To test whether CHC profiles differed between males of either wing morph, we first performed dimension reduction using principal components analysis (PCA) on male data only. JMP Trial 14.1.0 (SAS Institute Inc.) was used to draw a 3D scatterplot of the first three PCs. To assess statistical significance, we performed a MANOVA using all principal components with eigenvalue > 1.00 (n = 6). This indicated a highly significant difference among male morphs which formed the basis of QTL mapping described above. To visualise the difference between flatwing and normal-wing male CHC profiles with respect to female CHC profiles, we performed a discriminant function analysis (DFA) for all samples and all 26 peaks. DFA highlights the maximal difference between pre-defined groups, with maximum group differences indicated by the first DF axis. Statistical analyses of CHC data were done in SPSS (v.23).

Data Availability. Raw reads from Illumina and PacBio genome sequencing libraries, embryo RNAseq reads, RADseq reads used in the linkage map and QTL analyses, CHC phenotype data will be made publicly available upon acceptance. Custom scripts are available online at http://www.chirpbase.org if not stated otherwise.

Figures

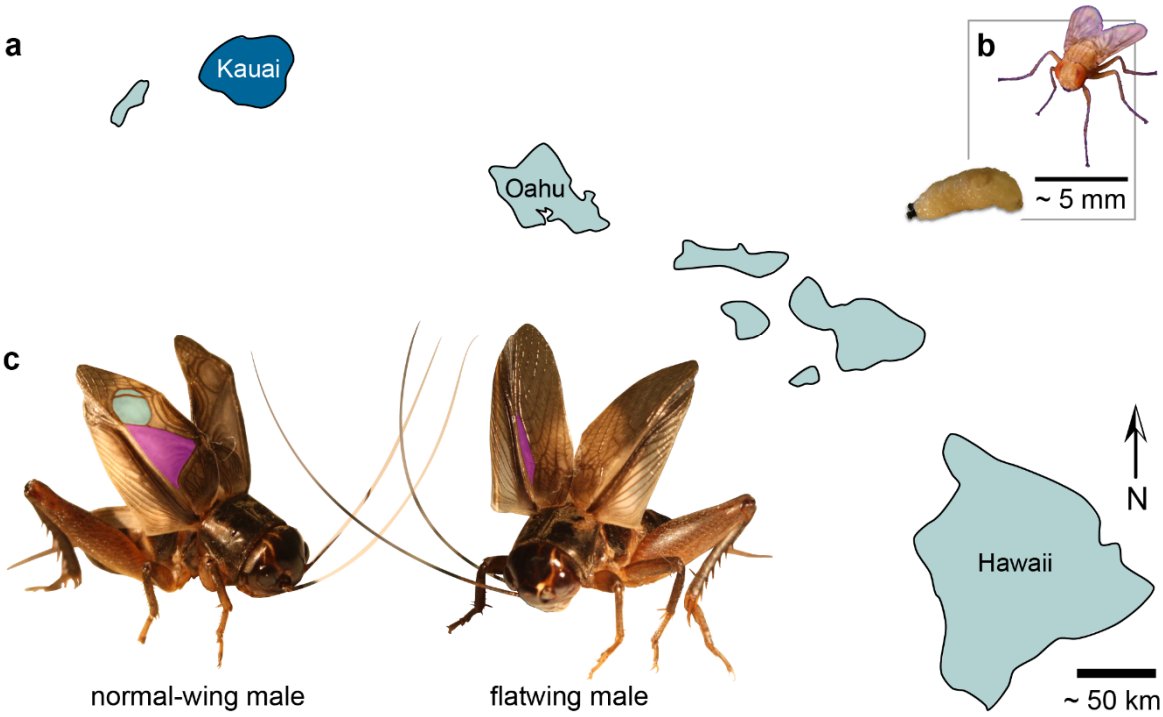

Fig. 1 | Rapid evolutionary loss of song in Hawaiian crickets. a, The field cricket *T. oceanicus* is thought to have migrated to the Hawaiian archipelago from other islands in Oceania, and is attacked by the fatal, acoustically-orienting parasitoid fly *Ormia ochracea* on Kauai, Oahu and Hawaii. We studied crickets from a population in Kauai, highlighted in dark blue, where parasitoid infestation rates have historically been highest. **b**, Adult female fly and mature parasitoid larva. Gravid female flies locate hosts by eavesdropping on singing male crickets, then they eject larvae that burrow into the host and consume its viscera before emerging to pupate. Infestation is fatal, and the flies exert significant natural selection against male song. **c**, Normal-wing males (left) of this field cricket species produce advertisement, courtship and aggressive songs by elevating and rubbing together forewings that bear specialised sound-producing venation. A toothed file on the right wing engages with a thickened ridge of tissue on the opposite, causing resonators to vibrate and produce sound. Two principal resonators are highlighted on this male's right forewing: the harp in purple and the mirror in turquoise. Flatwing males (right) have wings that are feminised and lack, or have severely reduced, resonators. They still make wing motions characteristic of singing despite the structural inability to produce sound[93], but their silence protects them from the fly[4]. The flatwing phenotype segregates as a single-locus mutation on the X chromosome, and 100% of males from the population studied on Kauai now exhibit flatwing morphology. (Photo credits: N.W. Bailey)

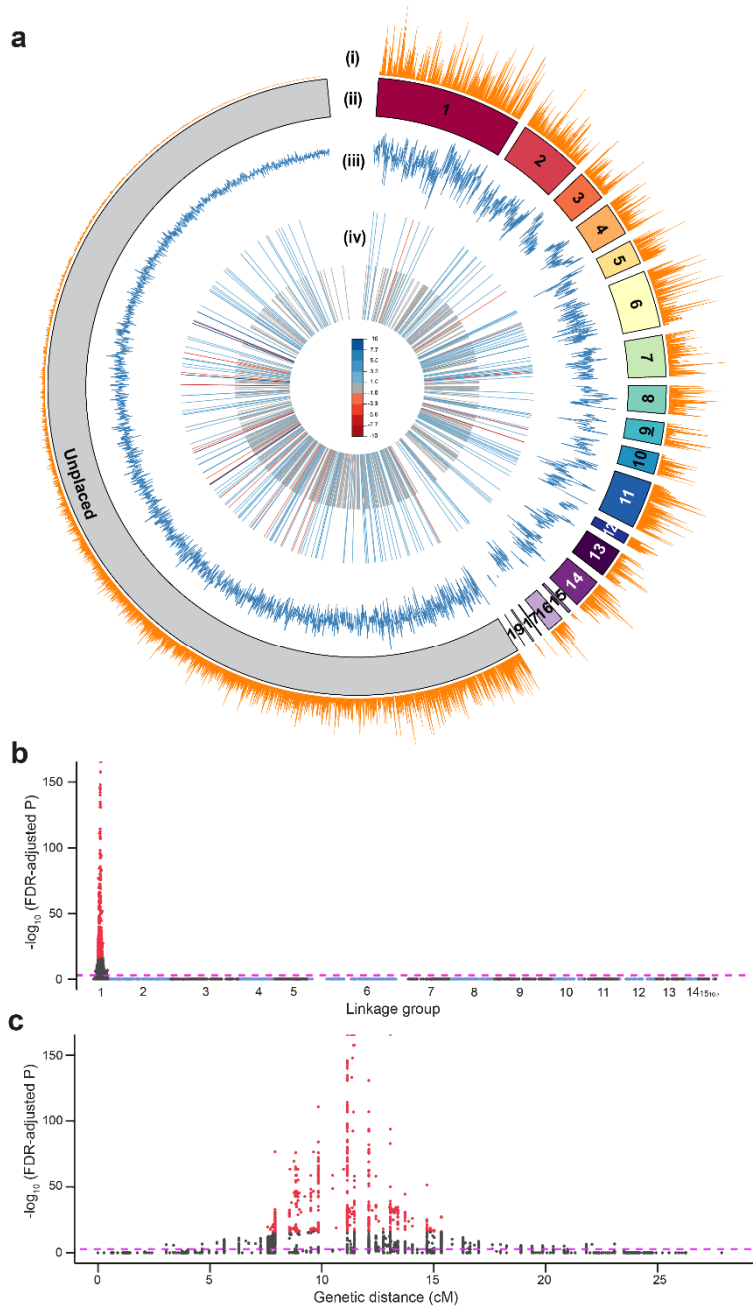

Fig. 2 | *Teleogryllus oceanicus* genome and regions associated with the flatwing phenotype. **a,** Circos plot providing an overview of the genome. Linkage groups (LGs) upon which genome scaffolds were anchored are shown in different colours, with unplaced scaffolds in gray. LG1 was identified as the X chromosome based on heterozygosity and coverage filters (see Main Text). Tracks (i): gene density, (ii): linkage group pseudomolecules, (iii): transposable element density, (iv): genes DE in the thoracic tissues of embryos homozygous for *flatwing* vs. *normal-wing* genotypes. Longer bars are DE genes for which $\log_2$FC > 1 between genotypes, and short grey bars are all other DE genes. Colours indicate the magnitude of upregulation (red) versus downregulation (blue) in *flatwing* compared to *normal-wing* embryos. **b,** Genome-wide Manhattan plot of the flatwing QTL. Alternating shades of grey and blue indicate different LGs. The horizontal dashed line indicates an FDR-corrected significance threshold of ($P < 0.001$), and the top 1% most significant QTL markers are plotted in red. **c,** Enlarged plot for LG1 (X chromosome) showing the flatwing-associated peak.

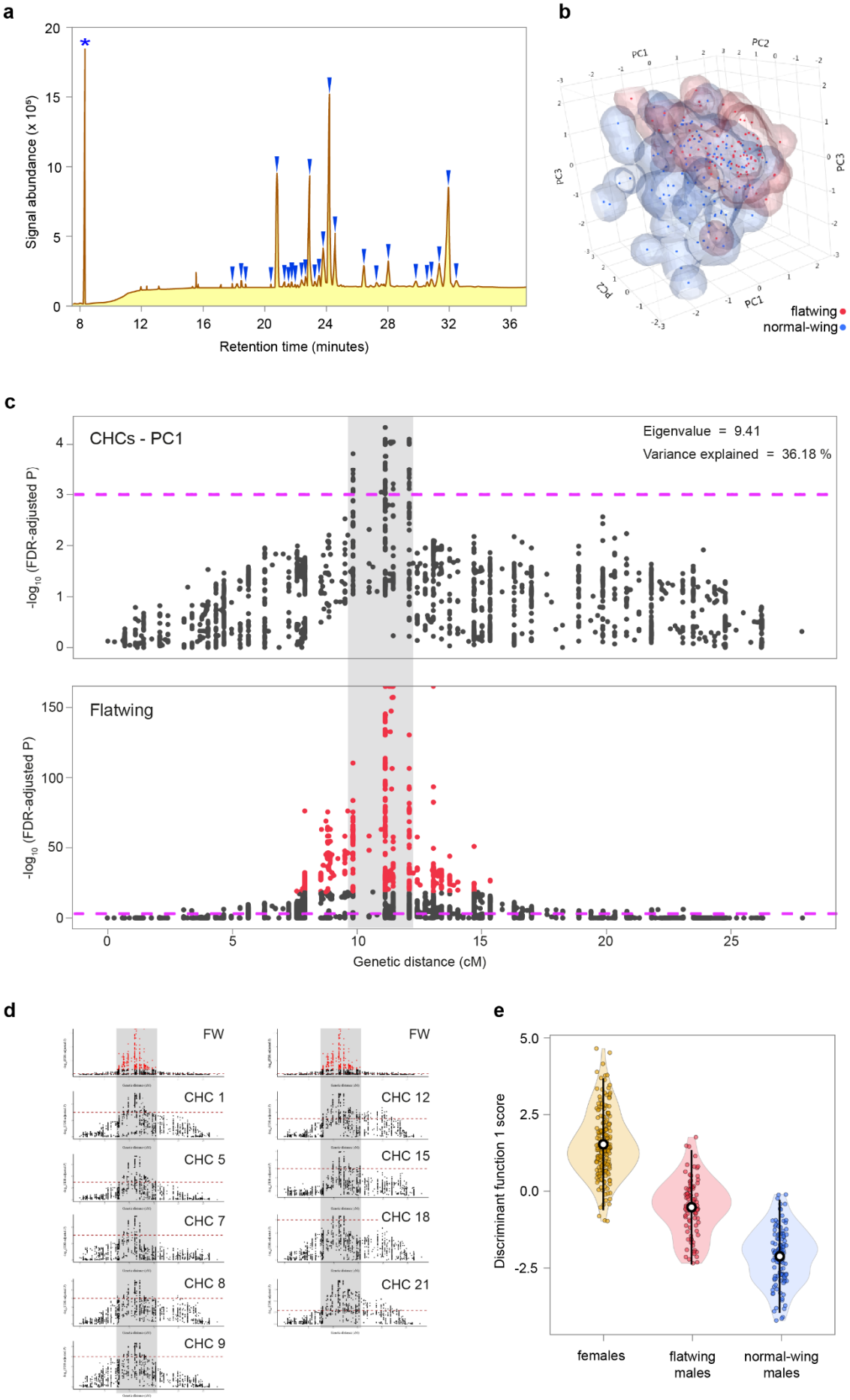

Fig. 3 | Pleiotropic effects of *flatwing* cause feminisation of chemical sexual signals. a, Diagram of a *T. oceanicus* cuticular hydrocarbon (CHC) chromatogram, with the 26 measured peaks indicated by blue wedges. The asterisk indicates the internal standard (pentadecane). **b,** Space-filling scatterplot of the first three principal components describing male CHC profiles, illustrating differences between flatwing and normal-wing males (variance explained for PC1: 35.18%, PC2: 10.14%, PC3: 9.58%). **c,** Comparison of QTL on the putative X chromosome for CHCs (top; first principal component mapped) and flatwing (bottom, same as Fig. 2C). Grey shading indicates the extent (in cM) of the CHC peak, showing overlap with the flatwing QTL. Dashed lines indicate FDR-corrected significance of $p < 0.001$, red points the top 1% significant flatwing QTL markers. Note the different y-axis scales. **d,** Univariate analyses revealed nine individual CHC components which also co-localised with flatwing. The original flatwing QTL is plotted at the top of each column. Grey shading spans the genetic region of co-localisation. Numbers refer to compounds indicated in **a**, and dashed lines indicate an FDR-corrected significance threshold of $p < 0.001$. **e,** Discriminant function scores describing variation in CHC profiles among female, flatwing male and normal-wing male mapping individuals. Discriminant function 1 explained 78.8% of the variance in CHC profiles between groups. Means ± 2 s.d. are indicated by open black-and-white circles and lines, respectively.

Extended Data Table 1 | *T. oceanicus* genome metrics

Maximum scaffold length (bp)	2,637,780	
Complete BUSCO (Ref total = 1,066)	1,001	
% complete BUSCO (genome)	93.9%	
% complete BUSCO (gene set)[a]	83.2%	
Scaffold metrics	**All contigs**	**Contigs > 1,000 bp**
Total bases (gb)	2,045,067,382	2,044,651,628
N50 (bp)	62,615	62,685
Sequences in N50	6,139	6,136
GC content (%)	40	40
Mean scaffold length (bp)	10,335	10,355
Sequencing library yields	**Read pairs**	**Yield (GB)**
Illumina TruSeq 180	277,076,641	55.42
Illumina TruSeq 300	243,927,180	48.79
Illumina TruSeq 600	238,275,727	47.66
Illumina TruSeq Nano 350	70,959,741	14.19
Illumina TruSeq Nano 550	63,415,263	12.68
Illumina Nextera mate-pair	229,431,023	45.89
PacBio RSII	5,771,779	21.74

[a] Final gene number identified in Extended Data Table 6

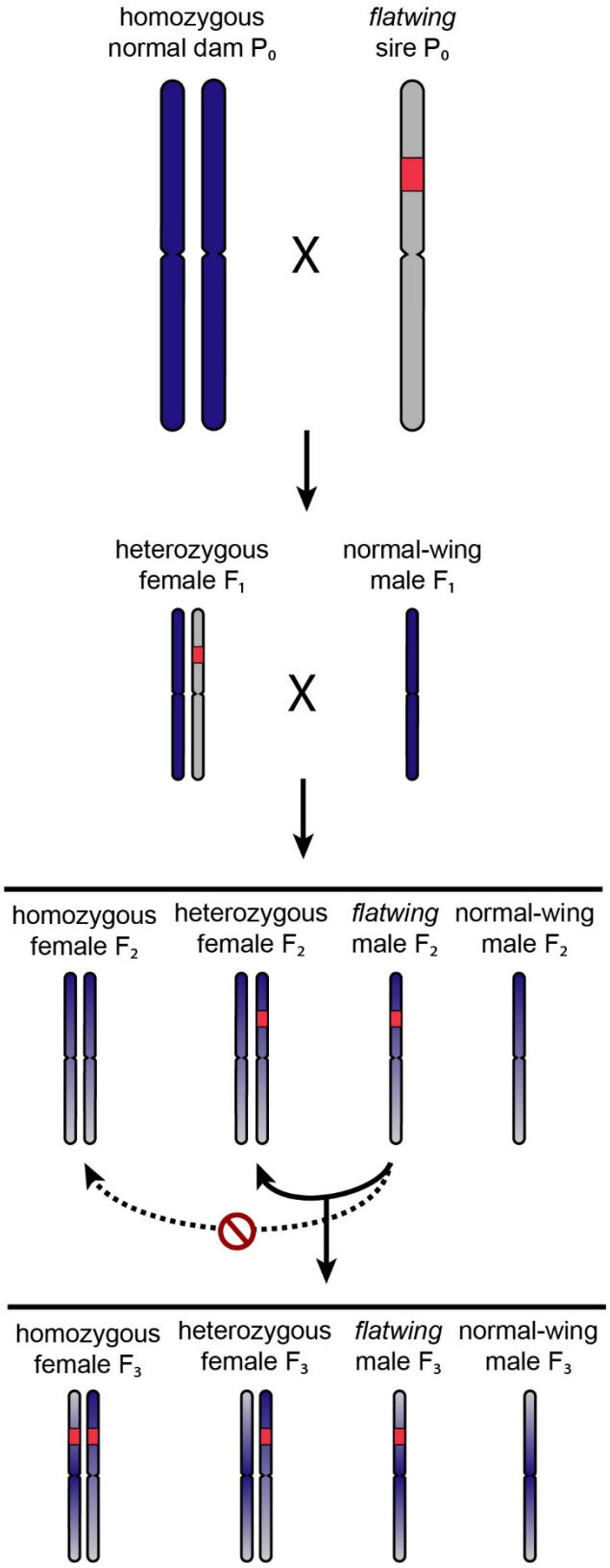

Extended Data Figure 1 | Cross design for linkage and QTL mapping. *Flatwing* segregates as a single-locus X-linked trait, so only X chromosomes are illustrated. A hypothetical *flatwing* locus is shaded in red. Females and males are XX/XO in *T. oceanicus*, so we performed three generations of crossing to enhance our ability to map *flatwing*. Homozygous *normal-wing* dams were obtained from a laboratory population of the same species originally derived from a population that has never contained *flatwing* (dark blue chromosomes). In the parental generation, these *normal-wing* dams were crossed to *flatwing* sires from Kauai (light grey chromosome, with hypothetical *flatwing* locus shaded in red). Dam genotypes were undetectable at generation F_2 due to *flatwing's* sex-limited expression, so only full-sib crosses for which the flatwing male phenotype segregated in the subsequent F_3 generation were retained for phenotyping and QTL mapping (solid arrows).

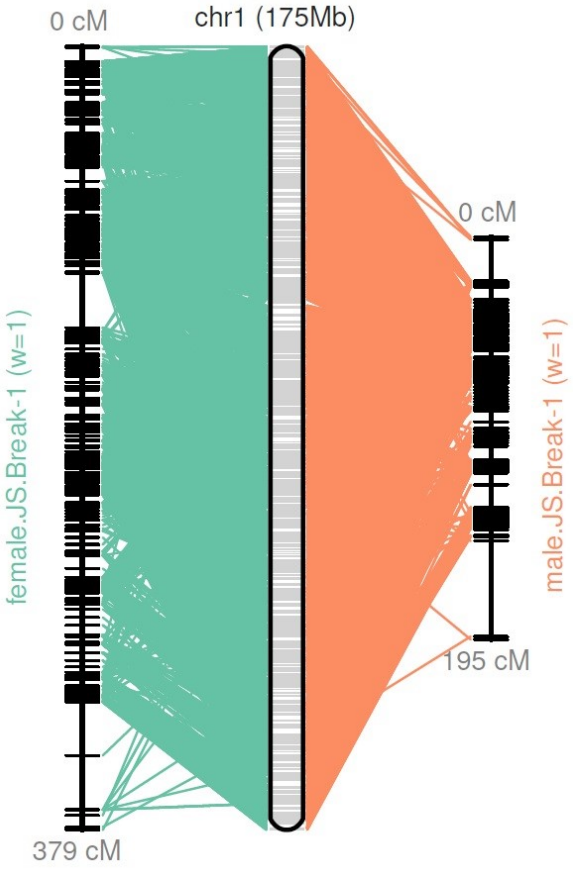

Extended Data Figure 2 | Reconstructed pseudomolecules for LG1 (putative X chromosome) using LOD5-supported markers. Female and male pseudomolecules are shown on the left and right, respectively, and lines connect the physical positions of markers on each pseudomolecule to map positions.

Extended Data Table 2 | List of chimeric scaffolds identified and corrected in the *T. oceanicus* genome

Chimeric scaffold	Coordinates		Corrected scaffold	Linkage group
	Start	Stop		
Contig112_pilon	1	280481	Contig112_pilon.1	LG13
Contig112_pilon	285560	415702	Contig112_pilon.2	LG4
Contig115174_pilon	1	4504	Contig115174_pilon.1	LG3
Contig115174_pilon	4505	9682	Contig115174_pilon.2	LG5
Contig11656_pilon	1	69510	Contig11656_pilon.1	LG3
Contig11656_pilon	71880	189927	Contig11656_pilon.2	LG2
Contig122717_pilon	1	791	Contig122717_pilon.1	LG12
Contig122717_pilon	792	1738	Contig122717_pilon.2	LG13
Contig12684_pilon	1	94718	Contig12684_pilon.1	LG14
Contig12684_pilon	94719	233653	Contig12684_pilon.2	LG16
Contig157093_pilon	1	21374	Contig157093_pilon.1	LG1
Contig157093_pilon	21375	29205	Contig157093_pilon.2	LG2
Contig16901_pilon	1	14926	Contig16901_pilon.1	LG16
Contig16901_pilon	18394	186701	Contig16901_pilon.2	LG11
Contig17374_pilon	1	391141	Contig17374_pilon.1	LG11
Contig17374_pilon	392712	614243	Contig17374_pilon.2	LG3
Contig19418_pilon	1	216097	Contig19418_pilon.1	LG10
Contig19418_pilon	220070	446236	Contig19418_pilon.2	LG12
Contig24478_pilon	1	10308	Contig24478_pilon.1	LG19
Contig24478_pilon	13057	232760	Contig24478_pilon.2	LG13
Contig25912_pilon	1	178241	Contig25912_pilon.1	LG12
Contig25912_pilon	180760	432977	Contig25912_pilon.2	LG11
Contig3004_pilon	1	113166	Contig3004_pilon.1	LG10
Contig3004_pilon	113846	201707	Contig3004_pilon.2	LG1
Contig30253_pilon	1	75616	Contig30253_pilon.1	LG6
Contig30253_pilon	75924	107012	Contig30253_pilon.2	LG10
Contig30890_pilon	1	42473	Contig30890_pilon.1	LG7
Contig30890_pilon	42474	357127	Contig30890_pilon.2	LG4
Contig32501_pilon	1	79400	Contig32501_pilon.1	LG8

Contig32501_pilon	81158	104315	Contig32501_pilon.2	LG5
Contig34163_pilon	1	276874	Contig34163_pilon.1	LG14
Contig34163_pilon	278116	477845	Contig34163_pilon.2	LG8
Contig34793_pilon	1	35174	Contig34793_pilon.1	LG13
Contig34793_pilon	35175	226445	Contig34793_pilon.2	LG4
Contig37346_pilon	1	181531	Contig37346_pilon.1	LG1
Contig37346_pilon	185444	510953	Contig37346_pilon.2	LG5
Contig44873_pilon	1	96939	Contig44873_pilon.1	LG3
Contig44873_pilon	100500	540225	Contig44873_pilon.2	LG2
Contig53403_pilon	1	162159	Contig53403_pilon.1	LG1
Contig53403_pilon	163594	231179	Contig53403_pilon.2	LG12
Contig6264_pilon	1	582129	Contig6264_pilon.1	LG1
Contig6264_pilon	582130	671930	Contig6264_pilon.2	LG16
Contig6264_pilon	675095	875693	Contig6264_pilon.3	LG1
Contig67999_pilon	1	75111	Contig67999_pilon.1	LG8
Contig67999_pilon	80918	230728	Contig67999_pilon.2	LG16
Contig7355_pilon	1	31398	Contig7355_pilon.1	LG4
Contig7355_pilon	31626	89218	Contig7355_pilon.2	LG7

Extended Data Table 3 | Summary statistics describing scaffold anchoring on *T. oceanicus* LOD5 linkage map markers

	Anchored	Oriented	Unplaced
Markers (unique)	104,713	88,665	741
Markers per Mb	143.9	154.5	0.6
Scaffolds	8,169	5,997	189,726
Scaffolds with 1 marker	686	0	187
Scaffolds with 2 markers	587	471	63
Scaffolds with 3 markers	578	368	37
Scaffolds with >=4 markers	6,318	5,158	50
Total bases	727,468,034 (35.6%)	573,790,325 (28.1%)	1,317,555,539 (64.4%)

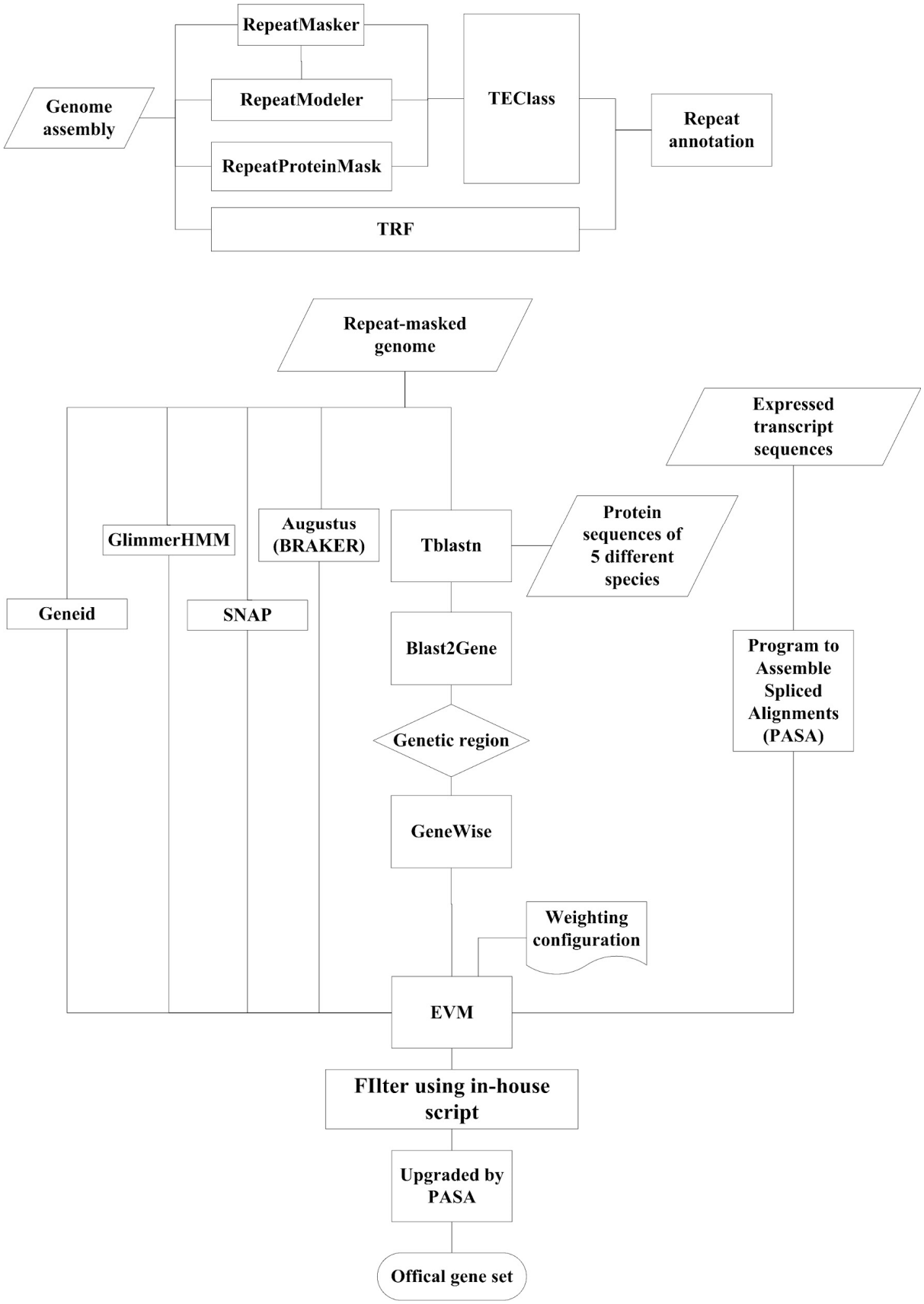

Extended Data Figure 3 | Workflow diagram of repeat annotation (top) and gene prediction (bottom) pipelines. Description of packages and parameters plus references are provided in the Methods section.

Extended Data Table 4 | Functional annotation of *T. oceanicus* genes

		Number	Proportion of all genes (%)
Total		19,157	-
Annotated	InterPro	12,318	64.3
	Swissprot	11,754	61.4
	TrEMBL	13,999	73.1
	NR	13,989	73.0
	Gene Ontology	13,177	68.7
	KEGG	9,579	50.0
	All annotated	14,367	75.0
Unknown		4,790	25.0

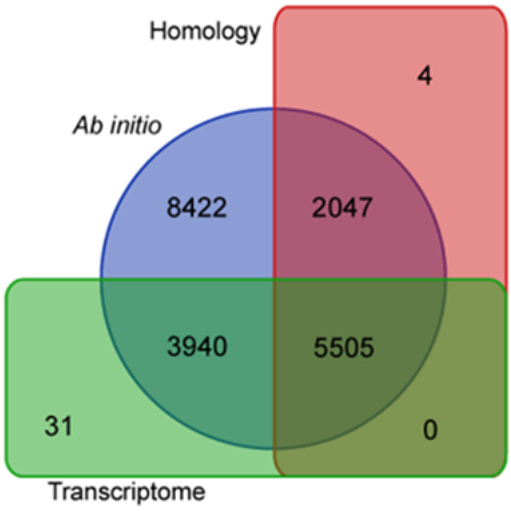

Extended Data Figure 4 | Venn diagram of genes predicted for *T. oceanicus* using different methods. Counts refer to the gene set that was obtained prior to final upgrade and filtering using PASA[71], so the total gene number above is slightly higher than the final gene set. A detailed description of each pipeline is presented in the Methods.

Extended Data Table 5 | Distribution of repetitive elements for each scaffolded *T. oceanicus* linkage group

Linkage group	Transposable elements (kb)	%	Rank[a]	Tandem repeats (kb)	%	Rank[a]	Combined (kb)	%	Rank[a]
LG1	65992	38.6	8	1832	1.1	20	67823	39.7	11
LG2	26518	35.7	17	1123	1.5	14	27641	37.2	17
LG3	12908	36.3	14	572	1.6	13	13480	37.9	14
LG4	16514	42.0	2	848	2.2	4	17362	44.2	2
LG5	10253	36.2	15	500	1.8	11	10753	37.9	15
LG6	23187	35.0	18	925	1.4	17	24113	36.4	18
LG7	17533	36.3	13	936	1.9	8	18469	38.2	13
LG8	12770	38.8	6	617	1.9	7	13387	40.7	6
LG9	9952	38.2	9	659	2.5	2	10611	40.7	7
LG10	9359	38.2	10	545	2.2	5	9904	40.5	8
LG11	18920	34.1	19	804	1.5	15	19724	35.6	19
LG12	4850	42.7	1	297	2.6	1	5148	45.4	1
LG13	12684	37.4	12	624	1.8	10	13308	39.2	12
LG14	12629	36.2	16	483	1.4	16	13112	37.6	16
LG15	1298	41.7	3	53	1.7	12	1351	43.5	3
LG16	6292	31.5	20	243	1.2	19	6535	32.7	20
LG17	337	39.5	5	10	1.2	18	347	40.7	5
LG18	699	38.2	11	42	2.3	3	741	40.5	9
LG19	3	27.4	21	0	0.4	21	3	27.8	21
Unplaced	526597	40.0	4	25416	1.9	6	552013	41.9	4
Total	789295	38.6	7	36531	1.8	9	825826	40.4	10

[a] Sorted by the proportion of repetitive elements in linkage groups, from most to fewest

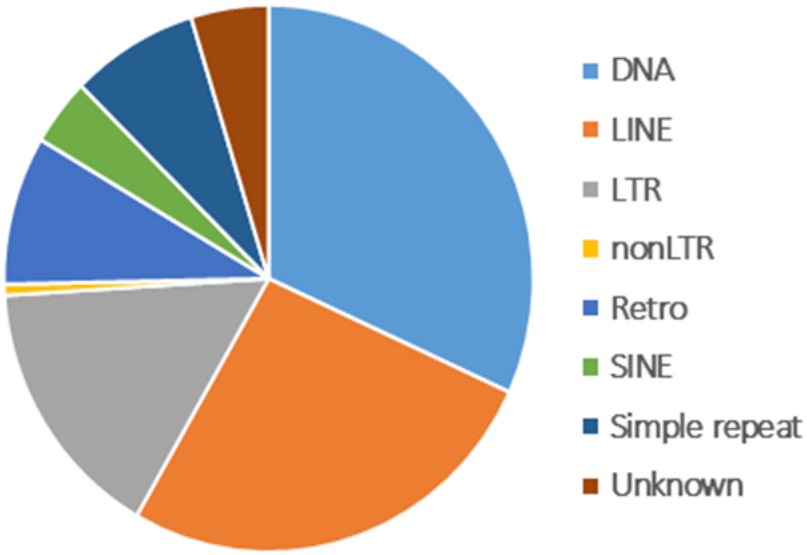

Extended Data Figure 5 | Proportions of eight major categories of transposable elements detected in the *T. oceanicus* genome.
DNA = DNA transposons
LTR = long terminal repeats
LINE = long interspersed nuclear elements
SINE = short interspersed nuclear elements
Retro = retrotransposon

Extended Data Table 6 | Comparison of gene features among ten insect species

Species	Genome assembly size (Gb)	Gene number	Single exon gene number	%	Average gene length	Average CDS length (bp)	Average exon number per transcript	Average exon length (bp)	Ref.
Field cricket									
Teleogryllus oceanicus	2.0	19,157	1,266	6.6	12,232	1,184	6.2	395	*this study*
Migratory locust									
Locusta migratoria	6.5	17,307	3,079	17.8	54,341[a]	1,160	5.8	201	[62]
American Cockroach									
Periplaneta americana	3.4	21,336	2,704	12.7	12,963[b]	-	4[b]	247[b]	[94]
Fruit fly									
Drosophila melanogaster	0.1	13,689	2,761	20.2	4,261	1,621	4.0	408	[64c]
Asian long-horned beetle									
Anoplophora glabripennis	0.7	16,200	1,194	7.4	18,596	1,744	6.6	265	[65]
Bed bug									
Cimex lectularius	0.7	13,751	1,410	10.3	29,076	1,846	10.2	265	[95]
Brown planthopper									
Nilaparvata lugens	1.1	21,442	2,179	10.2	22,015	1,440	6.9	289	[66]
Dampwood termite									
Zootermopsis nevadensis	0.5	15,129	370	2.4	24,927	1,890	9.4	365	[96]
Yellow fever mosquito									
Aedes aegypti	1.3	19,585	1,158	5.9	36,583	2,144	6.4	481	[97]
Asian Tiger mosquito									
Aedes albopictus	2.2	38,706	2,305	6.0	25,506	1,950	5.3	440	[98]

[a] Originally reported average transcript length
[b] Originally reported medians
[c] Adapted from[63]

Extended Data Table 7 | Transposable element classification in *T. oceanicus* contrasted with three published genomes

	T. oceanicus		*L. migratoria*[a]		*D. melanogaster*[a]		*H. sapiens*[a]	
Types	Repeat size (bp)	% of genome	Repeat size (bp)	% of genome	Repeat size (bp)	% of genome	Repeat size (bp)	% of genome
DNA	259181458	12.7	1,480,538,225	22.7	4,849,763	2.9	99,797,428	3.2
LINE	215705991	10.5	1,332,720,207	20.4	12,119,904	7.2	637,919,432	20.3
LTR	127951980	6.3	508,675,263	7.8	21,849,378	13.0	267,738,295	8.5
nonLTR	5233875	0.3	63,892,419	1.0	-	-	-	-
Retro	71828043	3.5	153,548,453	2.4	-	-	-	-
SINE	32344731	1.6	141,176,698	2.2	52,841	0.0	397,225,496	12.7
Simple repeat	63555524	3.1	13,026,240	0.2	2,733	0.0	26,240,511	0.8
Unknown	38615245	1.9	406,097,360	6.2	11,211,970	6.6	1,298,163	0.0
Total	789295269	38.6	3,840,808,141	58.9	50,785,143	30.0	1,434,373,137	46.0

DNA = DNA transposons
LTR = long terminal repeats
LINE = long interspersed nuclear elements
SINE = short interspersed nuclear elements
Retro = retrotransposon
[a] Data from[61]

Extended Data Table 8 | Thoracic gene expression variation between embryonic crickets carrying *flatwing* vs. *normal-wing* genotypes

Total number of genes passing expression filtering	10,961
Total DE genes	830
Up-regulated in *flatwing*	328
Down-regulated in *flatwing*	502
DE genes with $log_2FC > 1$	204
Up-regulated in *flatwing*	25
Down-regulated in *flatwing*	179

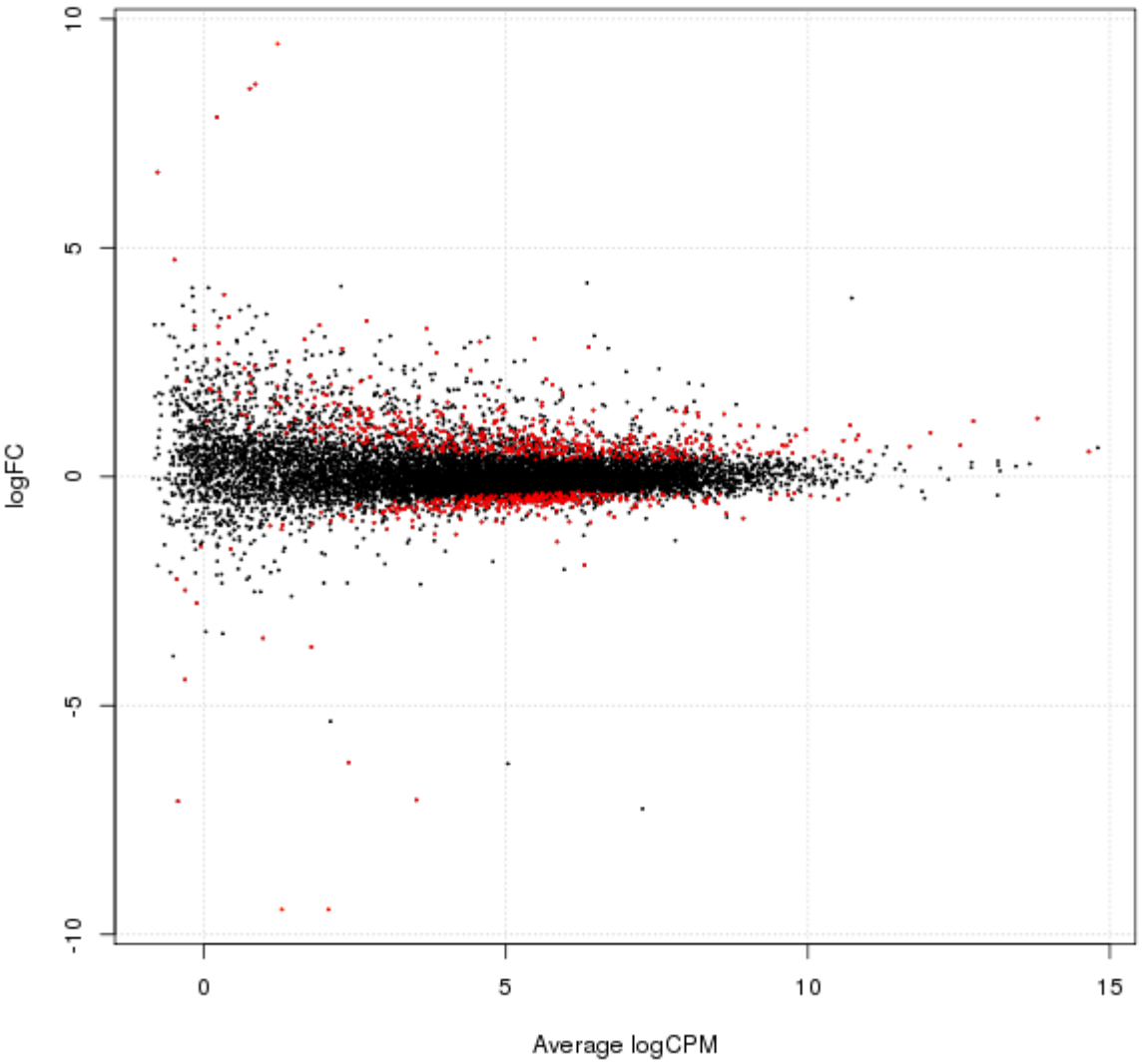

Extended Data Figure 6 | MA plot of thoracic genes DE between *T. oceanicus* embryos that were homozygous for *flatwing* vs. *normal-wing*. Red points indicate significantly differentially-expressed genes after filtering (see Methods), with positive values on the y-axis indicating genes downregulated in *flatwing* samples compared to *normal-wing* samples, and negative values indicating genes that are upregulated in *flatwing* samples. Log scales are base 2.

Extended Data Table 9 | GO analysis of thoracic DEGs between embryos carrying *flatwing* vs. *normal-wing* genotypes

GO	Type	Function	No. of DEGs	*P*-adj.
GO:0003824	molecular_function	catalytic activity	216	0.006
GO:0016787	molecular_function	hydrolase activity	80	0.027
GO:0044087	biological_process	regulation of cellular component biogenesis	20	0.004
GO:0051493	biological_process	regulation of cytoskeleton organization	12	0.023
GO:0090066	biological_process	regulation of anatomical structure size	12	0.009
GO:0097435	biological_process	supramolecular fiber organization	12	0.023
GO:0032535	biological_process	regulation of cellular component size	11	0.004
GO:0032956	biological_process	regulation of actin cytoskeleton organization	11	0.001
GO:0032970	biological_process	regulation of actin filament-based process	11	0.001
GO:1902903	biological_process	regulation of supramolecular fiber organization	11	0.002
GO:0043254	biological_process	regulation of protein complex assembly	10	0.035
GO:0110053	biological_process	regulation of actin filament organization	10	0.001
GO:0008064	biological_process	regulation of actin polymerization or depolymerization	8	0.006
GO:0030832	biological_process	regulation of actin filament length	8	0.006
GO:0030833	biological_process	regulation of actin filament polymerization	8	0.006
GO:0032271	biological_process	regulation of protein polymerization	8	0.015
GO:0015630	cellular_component	microtubule cytoskeleton	6	0.001
GO:0005248	molecular_function	voltage-gated sodium channel activity	5	0.004
GO:0010927	biological_process	cellular component assembly involved in morphogenesis	5	0.010
GO:0034706	cellular_component	sodium channel complex	4	0.007

Extended Data Table 10 | KEGG pathway enrichment of thoracic DEGs between embryos carrying *flatwing* vs. *normal-wing* genotypes

ID[a]	Pathway	No. of genes	*P*-value[b]	*P*-adj.[c]
map04520	Adherens junction	13	<0.001	0.025
map03030	DNA replication	9	0.001	0.264
map05100	Bacterial invasion of epithelial cells	9	0.007	0.408
map05130	Pathogenic Escherichia coli infection	9	0.005	0.408
map01100	Metabolic pathways	59	0.013	0.552
map04960	Aldosterone-regulated sodium reabsorption	5	0.012	0.552
map04064	NF-kappa B signaling pathway	5	0.021	0.687
map04711	Circadian rhythm - fly	3	0.024	0.715
map00230	Purine metabolism	18	0.038	0.744
map03430	Mismatch repair	5	0.035	0.744
map04111	Cell cycle - yeast	10	0.033	0.744
map04115	p53 signaling pathway	6	0.037	0.744
map04670	Leukocyte transendothelial migration	7	0.037	0.744
map04927	Cortisol synthesis and secretion	5	0.031	0.744
map03410	Base excision repair	5	0.044	0.765
map04022	cGMP-PKG signaling pathway	11	0.048	0.765
map04530	Tight junction	12	0.043	0.765

[a] Pathways describing human disease not shown

[b] Fisher's exact test

[c] FDR-corrected

Extended Data Table 11 | Top candidate genes associated with flatwing

Coordinates						
Scaffold	**Start**	**Stop**	**Gene ID**		**Description[a]**	**Source[b]**
Contig10220_pilon	78887	163134	TOT000182.1	YGD6	Zinc-type alcohol dehydrogenase-like protein C1773.06c	Top 1%
Contig11287_pilon	199864	215783	TOT001075.1	HNF4	Transcription factor HNF-4 homolog	Top 1%
Contig12423_pilon	12805	162659	TOT001854.1	OSM3	Osmotic avoidance abnormal protein 3	Top 1%
Contig12752_pilon	14326	68612	TOT002129.1	ROR1	Inactive tyrosine-protein kinase transmembrane receptor ROR1	Top 1%
Contig12919_pilon	275064	329308	TOT002239.1	CLOCK	Circadian locomotor output cycles protein kaput	Top 1% DEG
Contig13810_pilon	43734	77412	TOT002877.1	CRTAP	Cartilage-associated protein	Top 1%
Contig140_pilon	14528	100227	TOT003072.1	PP4R1	Serine/threonine-protein phosphatase 4 regulatory subunit 1	Top 1%
Contig17198_pilon	217974	328434	TOT004721.1	SCN60	Sodium channel protein 60E	Top 1%
Contig17198_pilon	398116	526355	TOT004722.1	SCN60	Sodium channel protein 60E	Top 1%
Contig17528_pilon	151965	161397	TOT004867.1	OBSTE	Protein obstructor-E	Kauai DEG
Contig17791_pilon	294998	303418	TOT005017.1	PKRA	Protein krasavietz	DEG QTL
Contig18506_pilon	5030	106086	TOT005335.1	STRN3	Striatin-3	Top 1%
Contig20777_pilon	197732	433721	TOT006213.1	COLL	Transcription factor collier	Top 1% BSA
Contig23358_pilon	266813	357642	TOT006927.1	E78C	Ecdysone-induced protein 78C (Eip78C)	Top 1%
Contig23647_pilon	61437	289082	TOT006991.1	RAVR1	Ribonucleoprotein PTB-binding 1	Top 1%
Contig24519_pilon	221508	332371	TOT007217.1	A0A167 WTZ1	Endo-1,3(4)-beta-glucanase	Top 1%
Contig24519_pilon	569981	635619	TOT007221.1	SEPIA	Pyrimidodiazepine synthase	Top 1%
Contig30320_pilon	33122	79411	TOT008755.1	PTPC1	Protein tyrosine phosphatase domain-containing protein 1	Top 1%
Contig3077_pilon	487713	492969	TOT008894.1	REXO4	RNA exonuclease 4	Top 1%
Contig31374_pilon	378769	413960	TOT009065.1	CPT2	Carnitine O-palmitoyltransferase 2, mitochondrial	Top 1%
Contig31374_pilon	461061	489320	TOT009067.1	FRM4B	FERM domain-containing protein 4B	Top 1%
Contig32190_pilon	94344	248306	TOT009274.1	RN207	RING finger protein 207	Top 1%
Contig35402_pilon	14084	125884	TOT010060.1	ABCG1	ATP-binding cassette sub-family G member 1	Top 1%
Contig37346_pilon.1	133394	180067	TOT010542.1	SCYL1	N-terminal kinase-like protein	Top 1%
Contig40107_pilon	150347	172207	TOT011176.1	THUM3	THUMP domain-containing protein 3	DEG, QTL
Contig4430_pilon	60074	108676	TOT012009.1	LAR	Tyrosine-protein phosphatase Lar	Top 1%
Contig4497_pilon	323	114981	TOT012126.1	MYO5A	Unconventional myosin-Va	Top 1%
Contig48084_pilon	4534	15580	TOT012711.1	KPEL	Serine/threonine-protein kinase pelle	Top 1%
Contig48322_pilon	73569	78934	TOT012764.1	CAH10	Carbonic anhydrase-related protein 10	Top 1%

Contig52923_pilon	4299	134158	TOT013504.1	RENT2	Regulator of nonsense transcripts 2	Top 1% DEG
Contig52923_pilon	172817	234071	TOT013505.1	NBL1	Neuroblastoma suppressor of tumorigenicity 1	Top 1%
Contig53931_pilon	135337	200203	TOT013689.1	TADBP	TAR DNA-binding protein 43	Top 1%
Contig55532_pilon	2641	6823	TOT013967.1	SOSSC	SOSSC_BOVIN	Top 1%
Contig5817_pilon	13001	94458	TOTO14395.1	A0A1B6LWD6	Uncharacterized protein	Top 1%
Contig6025_pilon	181847	338853	TOT014693.1	PAX6	Paired box protein Pax-6	Top 1%
Contig6181_pilon	7490	15461	TOT014894.1	MYCT	Proton myo-inositol cotransporter	Top 1%
Contig6371_pilon	72321	126646	TOT015146.5	GOGA4	Golgin subfamily A member 4	Top 1%
Contig6636_pilon	248427	279756	TOT015511.1	A0A067RPQ2	LRR domain-containing protein	Top 1%
Contig6636_pilon	332473	344815	TOT015512.1	IPR011011	Uncharacterized protein	Top 1%
Contig66512_pilon	19778	188429	TOT015537.1	LASP1	LIM and SH3 domain protein F42H10.3	Top 1% DEG
Contig6932_pilon	94582	114944	TOT015868.1	ABCB8	ATP-binding cassette sub-family B member 8, mitochondrial	Top 1%
Contig6932_pilon	132941	150338	TOT015869.1	APMAP	Adipocyte plasma membrane-associated protein	Top 1%
Contig7020_pilon	57223	96643	TOT015999.1	SPS1	Selenide, water dikinase	Top 1%
Contig7210_pilon	172512	326460	TOT016305.1	MYO	myoglianin	Top 1%
Contig7490_pilon	12720	16839	TOT016652.1	GCN5	Histone acetyltransferase GCN5	Top 1%
Contig8190_pilon	192630	256540	TOT017431.1	AT133	Probable cation-transporting ATPase 13A3	Top 1%
Contig82459_pilon	106133	176987	TOT017512.1	UNC89	Muscle M-line assembly protein unc-89	DEG QTL
Contig83863_pilon	1777	51856	TOT017662.1	A0A017RSC4	Uncharacterized protein	Top 1%
Contig92683_pilon	43257	76189	TOT018508.1	A0A0T6B8G7	Uncharacterized protein	Top 1%
Contig33215_pilon	67326	419738	TOT009518.1	PLXA4	Plexin-A4	QTL BSA
Contig43580_pilon	106377	137341	TOT011864.1	RNF41	E3 ubiquitin-protein ligase NRDP1	QTL BSA

[a] Functional descriptions and references provided in Main Text

[b] The criterion for inclusion as a top candidate was that a gene had to receive support for association with the flatwing phenotype from at least two of the following four sources:

QTL = portion of the gene was located within a 1 kb flanking region of a significantly-associated (FDR-corrected) marker in the flatwing QTL analysis

Top1% = portion of the gene was located within a 1 kb flanking region of a SNP in the top 1% of significantly-associated markers in the flatwing QTL analysis (Top1% candidates automatically received "QTL" support)

BSA = portion of the gene was located within a 1 kb flanking region of a significantly-associated marker from the previously-published bulked segregant analysis of Kauai flatwing males[7] which was also anchored to LG1

DEG = gene was significantly differentially expressed between pure-breeding *normal-wing* genotypes and *flatwing* genotypes, in embryonic thoracic tissue (track iv of Fig. 2a in Main Text)

Extended Data Table 12 | GO analysis of candidate flatwing-associated genes (CGs)

GO	Type	Function	No. of CGs	*P*-adj. (χ2 test)
GO:0010720	biological_process	positive regulation of cell development	3	<0.001
GO:0045597	biological_process	positive regulation of cell differentiation	3	0.002
GO:0060284	biological_process	regulation of cell development	3	0.042
GO:0003707	molecular_function	steroid hormone receptor activity	2	<0.001
GO:0009755	biological_process	hormone-mediated signaling pathway	2	0.006
GO:0030545	molecular_function	receptor regulator activity	2	0.035
GO:0043401	biological_process	steroid hormone mediated signaling pathway	2	0.002
GO:0045666	biological_process	positive regulation of neuron differentiation	2	0.040
GO:0048018	molecular_function	receptor ligand activity	2	0.022

Extended Data Table 13 | Identification of *Teleogryllus oceanicus* cuticular hydrocarbon profile peaks using gas chromatography - mass spectrometry

Peak[a]	Kováts retention index[b]	Identification	Diagnostic ions
standard		pentadecane	
1	2840	4MeC_{28}	365, 71
2	2893	10MeC_{28}	281, 155
3	2910	13MeC_{29}	252, 196
4	3028	$C_{30:1}$	434
5	3043	4MeC_{30}	436, 393, 71
6	3064	7,x-diMeC_{30}	365, 112
7	3075	unidentified	
8	3086	$C_{31:1}$	434
9	3110	11MeC_{31}	308, 168
10	3119	7,8MeC_{31}	364, 112
11	3130	7-C_{31}ene	434, 528[c], 145[c], 383[c]
12	3142	$C_{31:1}$	434
13	3152	$C_{31:2}$	432
14	3161	$C_{31:2}$	432
15	3174	$C_{31:2}$	432
16	3188	$C_{31:2}$	432
17	3242	4MeC_{32}	421, 71
18	3252	unidentified	
19	3268	$C_{32:2}$	446
20	3288	$C_{33:1}$	462
21	3331	$C_{33:1}$	462
22	3347	$C_{33:2}$	460
23	3355	$C_{33:2}$	460
24	3365	$C_{33:2}$	460
25	3379	3,x-$C_{33:2}$	460, 647[c], 89[c]
26	3391	$C_{33:2}$	460

[a] Peak identification is based on Table S4 of Pascoal et al. (2016)[83], reproduced here. The 26 quantified peaks are presented in sequential order in the table and in Fig. 3A of the main text.

[b] Calculation of the Kováts retention index using *n*-alkane standards (C_7 - C_{40}) is described in Majlát et al. (1974)[99]

[c] Ions used when identifying with dimethyl-disulphide derivation

Extended Data Table 14 | Principal components with eigenvalues > 1 from PCA on male CHC profiles; MANOVA results examine the effect of male morph on scores for each PC (multivariate model: Wilks' $\lambda = 0.517$, $F_{6,191} = 29.769$, $p < 0.001$).

Principal component	Eigenvalue	% Variance explained	$F_{1,196}$	P	R^2
1	9.408	36.18	25.885	<0.001	0.131
2	2.635	10.136	18.040	<0.001	0.092
3	2.490	9.576	21.454	<0.001	0.109
4	1.888	7.261	0.001	0.979	0.000
5	1.315	5.058	25.741	<0.001	0.131
6	1.020	3.925	4.079	0.043	0.021

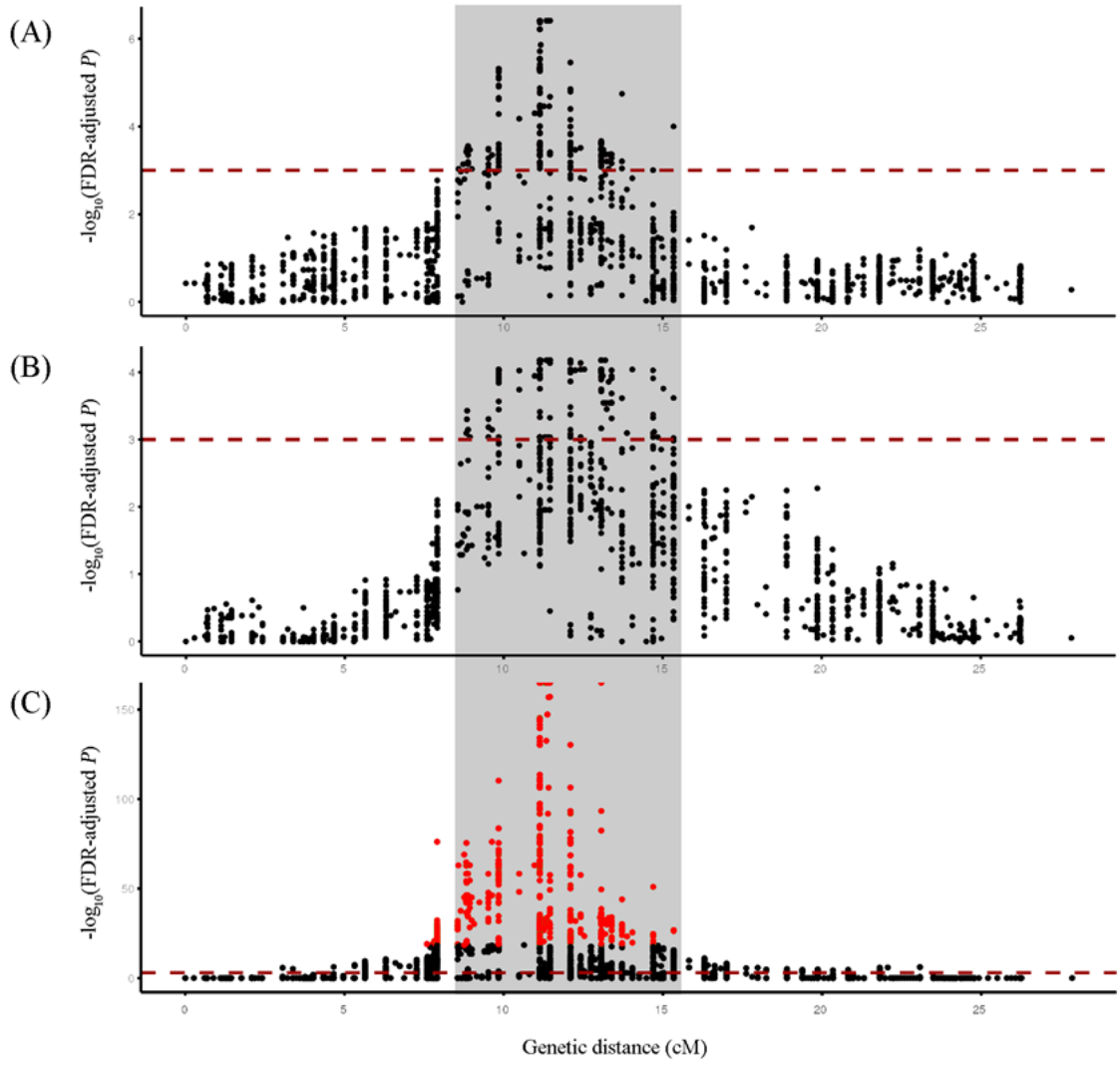

Extended Data Figure 7 | Genomic regions associated with different principal components describing male CHC profiles. Manhattan plot for LG1 (putative X chromosome) showing **a,** the PC4-associated QTL, **b,** PC6-associated QTL and **c,** the *flatwing* QTL for comparison. The horizontal dashed lines indicate FDR-corrected significance threshold of $P < 0.001$, and the top 1% most significant flatwing-associated QTL markers are plotted in red in **c**. The light grey rectangle spans the genetic region in which flatwing-associated markers and CHC principal component-associated markers co-localize.

Extended Data Table 15 | Candidate gene set associated with each CHC phenotype (individual or principal component) that yielded a significant QTL on the putative X (LG1), with the flatwing QTL for comparison

Coordinates			Gene ID	Trait													Description	
				Individual Compounds									PCs			Flat-wing		
Scaffold	Start	Stop		1	5	7	8	9	12	15	18	21	1	4	6			
Contig10220_pilon	78887	163134	TOT000182.1	√	√	√	√				√	√		√	√	√	YGD6	Zinc-type alcohol dehydrogenase-like protein C1773.06c
Contig11287_pilon	199864	215783	TOT001075.1	√	√	√	√	√	√	√	√	√	√	√	√	√	HNF4	Transcription factor HNF-4 homolog
Contig12423_pilon	12805	162659	TOT001854.1	√	√	√	√	√	√	√	√	√	√	√	√	√	OSM3	Osmotic avoidance abnormal protein 3
Contig14561_pilon	436209	450946	TOT003337.1								√						CAS	Transcription factor castor
Contig16800_pilon	571706	708271	TOT004499.1								√						SMAD3	Mothers against decapentaplegic homolog 3
Contig17198_pilon	217974	328434	TOT004721.1		√										√	√	SCN60	Sodium channel protein 60E
Contig17198_pilon	398116	526355	TOT004722.1	√				√			√			√		√	SCN60	Sodium channel protein 60E
Contig17589_pilon	46372	264973	TOT004897.1							√	√						SSBP3	Single-stranded DNA-binding protein 3
Contig17589_pilon	70840	324258	TOT004898.1							√	√						ATG10	Ubiquitin-like-conjugating enzyme ATG10
Contig17791_pilon	294998	303418	TOT005017.1	√	√						√	√				√	PKRA	Protein krasavietz
Contig18309_pilon	75967	136785	TOT005266.1		√												STA5B	Signal transducer and activator of transcription 5B
Contig191692_pilon	10444	19353	TOT005602.1								√						GNAI	Guanine nucleotide-binding protein G(i) subunit alpha
Contig20777_pilon	197732	433721	TOT006213.1	√	√					√	√	√	√	√		√	COLL	Transcription factor collier
Contig23454_pilon	18213	89940	TOT006946.1		√						√						ARD17	Arrestin domain-containing protein 17
Contig23647_pilon	61437	289082	TOT006991.1	√	√	√	√				√	√		√	√	√	RAVR1	Ribonucleoprotein PTB-binding 1
Contig24519_pilon	569981	635619	TOT007221.1								√					√	SEPIA	Pyrimidodiazepine synthase
Contig27628_pilon	259968	507152	TOT008051.1								√						PROH3	Prohormone-3
Contig29117_pilon	70169	396634	TOT008443.1		√	√	√				√						CCKAR	Cholecystokinin receptor type A
Contig29877_pilon	36855	181557	TOT008655.1		√												E41LA	Band 4.1-like protein 4A
Contig3077_pilon	487713	492969	TOT008894.1	√	√	√	√	√	√	√	√	√	√	√	√	√	REXO4	RNA exonuclease 4
Contig3077_pilon	528735	564924	TOT008896.1		√												P4K2B	Phosphatidylinositol 4-kinase type 2
Contig31374_pilon	461061	489320	TOT009067.1	√	√	√	√	√	√	√	√	√	√	√	√	√	FRM4B	FERM domain-containing protein 4B
Contig32190_pilon	94344	248306	TOT009274.1	√	√	√	√				√	√		√	√	√	RN207	RING finger protein 207
Contig3429_pilon	122631	136033	TOT009790.1	√							√						A0A1B6JV12	Uncharacterized protein
Contig3536_pilon	221796	347378	TOT010046.1		√						√						GNAO	Guanine nucleotide-binding protein G(o) subunit alpha
Contig35402_pilon	14084	125884	TOT010060.1		√	√					√			√	√	√	ABCG1	ATP-binding cassette sub-family G member 1
Contig3552_pilon	175659	203623	TOT010094.1		√						√						OSBL9	Oxysterol-binding protein-related protein 9
Contig37346_pilon.1	133394	180067	TOT010542.1	√	√	√	√	√	√	√	√	√	√	√	√	√	SCYL1	N-terminal kinase-like protein
Contig40569_pilon	70324	81832	TOT011293.1	√							√						NXT1	NTF2-related export protein
Contig43774_pilon	63974	228355	TOT011905.1								√						HMCN1	Hemicentin-1
Contig4430_pilon	60074	108676	TOT012009.1	√	√	√				√	√	√	√			√	LAR	Tyrosine-protein phosphatase Lar
Contig4451_pilon	20121	45182	TOT012039.1		√												LAR4	La-related protein Larp4B
Contig48084_pilon	4534	15580	TOT012711.1		√						√					√	KPEL	Serine/threonine-protein kinase pelle
Contig48322_pilon	73569	78934	TOT012764.1								√					√	CAH10	Carbonic anhydrase-related protein 10
Contig5051_pilon	34769	44241	TOT013154.1								√						CMYA5	Cardiomyopathy-associated protein 5

Contig52923_pilon	172817	234071	TOT013505.1	√	√	√	√			√	√	√		√	√	√	NBL1	Neuroblastoma suppressor of tumorigenicity 1
Contig53931_pilon	135337	200203	TOT013689.1	√	√	√				√	√	√		√		√	TADBP	TAR DNA-binding protein 43
Contig5490_pilon	190540	238169	TOT013863.1		√						√						UNC89	Muscle M-line assembly protein unc-89
Contig5490_pilon	145320	153034	TOT013873.1								√						A0A067RCZ8	Uncharacterized protein
Contig5542_pilon	24715	684526	TOT013934.1		√						√						GALT2	Polypeptide N-acetylgalactosaminyltransferase 2
Contig55532_pilon	2641	6823	TOT013967.1		√						√					√	SOSSC	SOSS complex subunit C
Contig5817_pilon	13001	94458	TOT014395.1			√					√					√	A0A1B6LWD6	Uncharacterized protein
Contig6025_pilon	181847	338853	TOT014693.1	√	√	√	√				√	√		√	√	√	PAX6	Paired box protein Pax-6
Contig6181_pilon	7490	15461	TOT014894.1		√						√				√	√	MYCT	Proton myo-inositol cotransporter
Contig6371_pilon	72321	126646	TOT015146.5	√	√	√				√	√	√		√	√	√	GOGA4	Golgin subfamily A member 4
Contig63833_pilon	68993	231055	TOT015158.1								√						HUWE1	E3 ubiquitin-protein ligase HUWE1
Contig6636_pilon	248427	279756	TOT015511.1	√	√	√				√	√	√		√		√	A0A067RPQ2	LRR domain-containing protein
Contig66512_pilon	19778	188429	TOT015537.1	√	√					√	√	√		√		√	LASP1	LIM and SH3 domain protein F42H10.3
Contig6932_pilon	94582	114944	TOT015868.1		√						√					√	ABCB8	ATP-binding cassette sub-family B member 8, mitochondrial
Contig6932_pilon	132941	150338	TOT015869.1		√						√					√	APMAP	Adipocyte plasma membrane-associated protein
Contig7210_pilon	172512	326460	TOT016305.1	√	√	√				√	√	√	√	√		√	MYO	myoglianin
Contig745_pilon	6060	59826	TOT016600.1								√						E41L5	Band 4.1-like protein 5
Contig7490_pilon	12720	16839	TOT016652.1	√	√	√				√	√	√		√	√	√	GCN5	Histone acetyltransferase GCN5
Contig8263_pilon	12087	12734	TOT017545.1		√		√				√			√	√		TWF	Twinfilin
Contig92683_pilon	43257	76189	TOT018508.1	√	√	√	√	√	√	√	√	√	√	√	√	√	A0A0T6B8G7	Uncharacterized protein

Extended Data Table 16 | Allele replacement table for identifying the X chromosome in the *T. oceanicus* linkage map

Dam	Sire	Sire assumed	Sire rewrite	male current	male rewrite	male current	male rewrite
0/1	0/0	0/.	0/2	0/0	0/2	1/1	1/2
0/1	1/1	1/.	1/2	0/0	0/2	1/1	1/2
0/1	2/2	2/.	NA	-	-	-	-
0/2	0/0	0/.	0/1	0/0	0/1	2/2	1/2
0/2	1/1	1/.	NA	-	-	-	-
0/2	2/2	2/.	2/1	0/0	0/1	2/2	2/1
1/2	0/0	0/.	NA	-	-	-	-
1/2	1/1	1/.	1/3	1/1	1/3	2/2	2/3
1/2	2/2	2/.	2/3	1/1	1/3	2/2	2/3

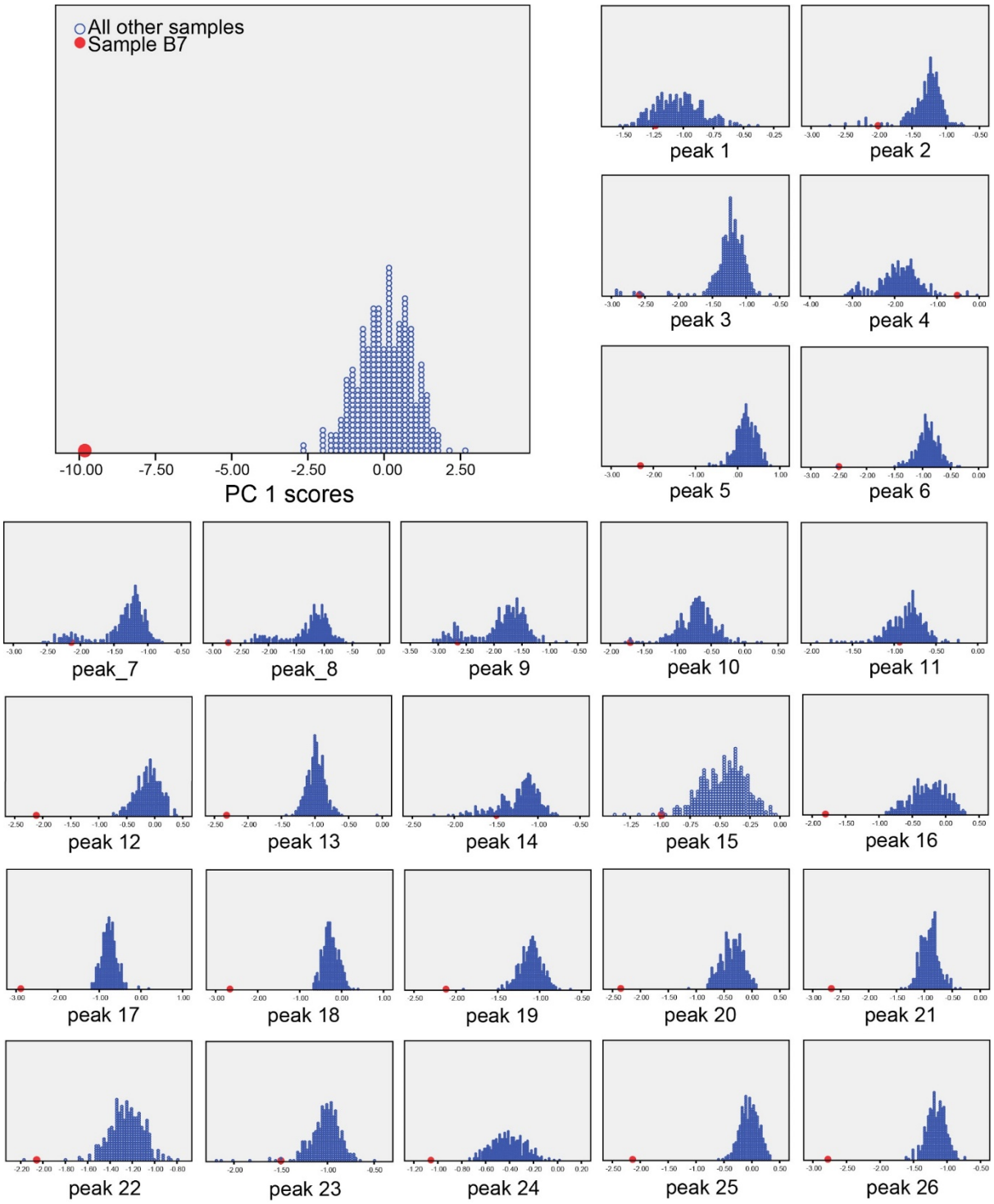

Extended Data Figure 8 | Histograms illustrating the identification of a CHC sample outlier. Sample B7, a normal-wing male, is indicated by the enlarged red dot in each plot. The sample was observed on visual inspection to deviate substantially from the distribution of principal component 1 scores for all other mapping individuals. Further inspection revealed this also to be the case in the majority of cases when the sample was assessed for each CHC peak individually. It was thus excluded from further analysis.

Acknowledgements The Natural Environment Research Council provided funding to N.W.B. (NE/G014906/1, NE/L011255/1), and to N.W.B. and M.G.R. (NE/1027800/1). Sequencing support was provided by Edinburgh Genomics and the Centre for Genomic Research at the University of Liverpool. Bioinformatics resources at St Andrews were funded by a Wellcome Trust ISSF award (105621/Z/14/Z). Support from the China Scholarship Council (201703780018) to X.Z. is gratefully acknowledged. The Biotechnology and Biological Sciences Research Council provided support to M.B. which aided in the development of ChirpBase (BB/K020161/1). We thank J. Kenny for NGS sequencing advice; Y. Fang for read processing; R. Fallon for bioinformatics assistance; J.Q. Liu and K. Wang for advice regarding gene prediction pipelines; J. Bastiaansen and P. Gienapp for assistance with ASReml, W.V. Bailey, B. Gray, J.T. Rotenberry, S. Vardy and M. Zuk for assistance in the field; D. Forbes, A. Grant and T. Sneddon for assistance in the laboratory; C. Mitchell for assistance with CHC analyses.

Author contributions N.W.B. conceived and led the study. S.P., K.G., M.B., M.G.R. and N.W.B. designed experiments. S.P. led data collection. S.P. did genetic crosses and wet lab work. S.P., J.E.R., X.Z., T.C., E.L., X.L., J.H., J.G.R., B.L.S., U.T. and N.W.B. performed analyses. M.B., R.J.C., S.J., E.L., M.B. and N.W.B. designed ChirpBase. N.W.B. led manuscript writing. S.P., J.E.R., X.Z., E.L., M.B., M.G.R. and N.W.B contributed to writing.

Competing interests The authors declare no competing interests.

References

1. Wiens, J. J. Widespread loss of sexually selected traits: how the peacock lost its spots. *Trends in Ecology & Evolution* **16**, 517-523 (2001).
2. Whiting, M. F., Bradler, S. & Maxwell, T. Loss and recovery of wings in stick insects. *Nature* **421**, 264-267 (2003).
3. Nadeau, J. H. *et al.* Pleiotropy, homeostasis, and functional networks based on assays of cardiovascular traits in genetically randomized populations. *Genome Res* **13**, 2082-2091 (2003).
4. Zuk, M., Rotenberry, J. T. & Tinghitella, R. M. Silent night: adaptive disappearance of a sexual signal in a parasitized population of field crickets. *Biol Lett* **2**, 521-524 (2006).
5. Zuk, M., Bailey, N. W., Gray, B. & Rotenberry, J. T. Sexual signal loss: The link between behaviour and rapid evolutionary dynamics in a field cricket. *J Anim Ecol* **87**, 623-633 (2018).
6. Tinghitella, R. M. Rapid evolutionary change in a sexual signal: genetic control of the mutation 'flatwing' that renders male field crickets (Teleogryllus oceanicus) mute. *Heredity* **100**, 261-267 (2008).
7. Pascoal, S. *et al.* Rapid convergent evolution in wild crickets. *Curr Biol* **24**, 1369-1374 (2014).
8. Fisher, R. *The Genetical Theory of Natural Selection*. 1st edn, (The Clarendon Press, 1930).
9. Orr, H. A. The genetic theory of adaptation: a brief history. *Nat Rev Genet* **6**, 119-127 (2005).
10. Hartley, C. J. *et al.* Amplification of DNA from preserved specimens shows blowflies were preadapted for the rapid evolution of insecticide resistance. *Proc Natl Acad Sci U S A* **103**, 8757-8762 (2006).
11. Raymond, M., Berticat, C., Weill, M., Pasteur, N. & Chevillon, C. Insecticide resistance in the mosquito *Culex pipiens*: what have we learned about adaptation? *Genetica* **112-113**, 287-296 (2001).
12. van't Hof, A. E., Edmonds, N., Dalikova, M., Marec, F. & Saccheri, I. J. Industrial melanism in British peppered moths has a singular and recent mutational origin. *Science* **332**, 958-960 (2011).
13. Van't Hof, A. E. *et al.* The industrial melanism mutation in British peppered moths is a transposable element. *Nature* **534**, 102-105 (2016).
14. True, J. R. Insect melanism: the molecules matter. *Trends in Ecology & Evolution* **18**, 640-647 (2003).
15. Challis, R. J., Kumar, S., Stevens, L. & Blaxter, M. GenomeHubs: simple containerized setup of a custom Ensembl database and web server for any species. *Database (Oxford)* **2017**,

doi:10.1093/database/bax039 (2017).
16. Snodgrass, R. E. *Principles of Insect Morphology* (Cornell University Press, 1993).
17. De Celis, J. F. Pattern formation in the *Drosophila* wing: The development of the veins. *Bioessays* **25**, 443-451 (2003).
18. Hatini, V., Kula-Eversole, E., Nusinow, D. & Del Signore, S. J. Essential roles for stat92E in expanding and patterning the proximodistal axis of the *Drosophila* wing imaginal disc. *Dev Biol* **378**, 38-50 (2013).
19. Vervoort, M., Crozatier, M., Valle, D. & Vincent, A. The COE transcription factor Collier is a mediator of short-range Hedgehog-induced patterning of the *Drosophila* wing. *Curr Biol* **9**, 632-639 (1999).
20. Hevia, C. F. & de Celis, J. F. Activation and function of TGFbeta signalling during *Drosophila* wing development and its interactions with the BMP pathway. *Dev Biol* **377**, 138-153 (2013).
21. Bicocca, V. T. *et al.* Crosstalk between ROR1 and the Pre-B cell receptor promotes survival of t(1;19) acute lymphoblastic leukemia. *Cancer Cell* **22**, 656-667 (2012).
22. Carvajal-Gonzalez, J. M., Mulero-Navarro, S., Smith, M. & Mlodzik, M. A novel Frizzled-based screening tool identifies genetic modifiers of planar cell polarity in *Drosophila* wings. *G3 (Bethesda)* **6**, 3963-3973 (2016).
23. Adler, P. N. The frizzled/stan pathway and planar cell polarity in the *Drosophila* wing. *Curr Top Dev Biol* **101**, 1-31 (2012).
24. Wu, C. *et al.* Pelle modulates dFoxO-mediated cell death in *Drosophila*. *Plos Genet* **11**, e1005589, doi:10.1371/journal.pgen.1005589 (2015).
25. Carre, C., Szymczak, D., Pidoux, J. & Antoniewski, C. The histone H3 acetylase dGcn5 is a key player in *Drosophila melanogaster* metamorphosis. *Mol Cell Biol* **25**, 8228-8238 (2005).
26. Okada, H., Ebhardt, H. A., Vonesch, S. C., Aebersold, R. & Hafen, E. Proteome-wide association studies identify biochemical modules associated with a wing-size phenotype in *Drosophila melanogaster*. *Nat Commun* **7**, 12649, doi:10.1038/ncomms12649 (2016).
27. Tregenza, T. & Wedell, N. Definitive evidence for cuticular pheromones in a cricket. *Anim Behav* **54**, 979-984 (1997).
28. Thomas, M. L. & Simmons, L. W. Sexual selection on cuticular hydrocarbons in the Australian field cricket, *Teleogryllus oceanicus*. *BMC Evol Biol* **9**, 162, doi:10.1186/1471-2148-9-162 (2009).
29. Thomas, M. L. & Simmons, L. W. Cuticular hydrocarbons influence female attractiveness to males in the Australian field cricket, *Teleogryllus oceanicus*. *J Evol Biol* **23**, 707-714 (2010).
30. Simmons, L. W., Thomas, M. L., Gray, B. & Zuk, M. Replicated evolutionary divergence in the cuticular hydrocarbon profile of male crickets associated with the loss of song in the Hawaiian archipelago. *J Evol Biol* **27**, 2249-2257 (2014).
31. Gray, B., Bailey, N. W., Poon, M. & Zuk, M. Multimodal signal compensation: do field crickets shift sexual signal modality after the loss of acoustic communication? *Animal behaviour* **93**, 243-248 (2014).
32. Dugatkin, L. A. *Principles of Animal Behavior*. 2nd edn, (W. W. Norton & Company, 2008).
33. Bank, C., Hietpas, R. T., Wong, A., Bolon, D. N. & Jensen, J. D. A bayesian MCMC approach to assess the complete distribution of fitness effects of new mutations: uncovering the potential for adaptive walks in challenging environments. *Genetics* **196**, 841-852 (2014).
34. Pascoal, S. *et al.* Rapid evolution and gene expression: a rapidly evolving Mendelian trait that silences field crickets has widespread effects on mRNA and protein expression. *J Evol Biol* **29**, 1234-1246 (2016).
35. Bailey, N. W., Gray, B. & Zuk, M. Acoustic experience shapes alternative mating tactics and reproductive investment in male field crickets. *Curr Biol* **20**, 845-849 (2010).
36. Pascoal, S. *et al.* Increased socially mediated plasticity in gene expression accompanies rapid adaptive evolution. *Ecol Lett* **21**, 546-556 (2018).
37. Kupper, C. *et al.* A supergene determines highly divergent male reproductive morphs in the ruff. *Nat Genet* **48**, 79-83 (2016).
38. Joag, R. *et al.* Transcriptomics of intralocus sexual conflict: Gene expression patterns in females change in response to selection on a male secondary sexual trait in the bulb mite. *Genome Biol Evol* **8**, 2351-2357 (2016).
39. Martin, M. Cutadapt removes adapter sequences from high-throughput sequencing reads. *EMBnet. journal* **17**, pp. 10-12 (2011).
40. Heo, Y., Wu, X. L., Chen, D., Ma, J. & Hwu, W. M. BLESS: bloom filter-based error correction solution

for high-throughput sequencing reads. *Bioinformatics* **30**, 1354-1362 (2014).
41. Rognes, T., Flouri, T., Nichols, B., Quince, C. & Mahe, F. VSEARCH: a versatile open source tool for metagenomics. *PeerJ* **4**, e2584, doi:10.7717/peerj.2584 (2016).
42. Kajitani, R. *et al.* Efficient de novo assembly of highly heterozygous genomes from whole-genome shotgun short reads. *Genome Res* **24**, 1384-1395 (2014).
43. English, A. C. *et al.* Mind the gap: upgrading genomes with Pacific Biosciences RS long-read sequencing technology. *PLoS One* **7**, e47768, doi:10.1371/journal.pone.0047768 (2012).
44. Walker, B. J. *et al.* Pilon: an integrated tool for comprehensive microbial variant detection and genome assembly improvement. *PLoS One* **9**, e112963, doi:10.1371/journal.pone. 0112963 (2014).
45. Simao, F. A., Waterhouse, R. M., Ioannidis, P., Kriventseva, E. V. & Zdobnov, E. M. BUSCO: assessing genome assembly and annotation completeness with single-copy orthologs. *Bioinformatics* **31**, 3210-3212 (2015).
46. Tarailo-Graovac, M. & Chen, N. Using RepeatMasker to identify repetitive elements in genomic sequences. *Curr Protoc Bioinformatics* **Chapter 4**, Unit 4 10, doi:10.1002/ 0471250953.bi0410s25 (2009).
47. Price, A. L., Jones, N. C. & Pevzner, P. A. De novo identification of repeat families in large genomes. *Bioinformatics* **21 Suppl 1**, i351-358, doi:21/suppl_1/i351 (2005).
48. Hubley, R. *et al.* The Dfam database of repetitive DNA families. *Nucleic Acids Res* **44**, D81-89, doi:10.1093/nar/gkv1272(2016).
49. Bao, W., Kojima, K. K. & Kohany, O. Repbase Update, a database of repetitive elements in eukaryotic genomes. *Mob DNA* **6**, 11, doi:10.1186/s13100-015-0041-9 (2015).
50. Boratyn, G. M. *et al.* Domain enhanced lookup time accelerated BLAST. *Biol Direct* **7**, 12, doi:10.1186/1745-6150-7-12 (2012).
51. Smit, A., Hubley, R. & Green, P. *RepeatMasker Open-4.0*, <http://www.repeatmasker.org> (2013-2015).
52. Abrusan, G., Grundmann, N., DeMester, L. & Makalowski, W. TEclass--a tool for automated classification of unknown eukaryotic transposable elements. *Bioinformatics* **25**, 1329-1330 (2009).
53. Benson, G. Tandem repeats finder: a program to analyze DNA sequences. *Nucleic Acids Res* **27**, 573-580 (1999).
54. Korf, I. Gene finding in novel genomes. *BMC Bioinformatics* **5**, 59, doi:10.1186/1471-2105-5-59 (2004).
55. Majoros, W. H., Pertea, M. & Salzberg, S. L. TigrScan and GlimmerHMM: two open source ab initio eukaryotic gene-finders. *Bioinformatics* **20**, 2878-2879 (2004).
56. Blanco, E., Parra, G. & Guigo, R. Using geneid to identify genes. *Curr Protoc Bioinformatics* **Chapter 4**, Unit 4 3, doi:10.1002/0471250953.bi0403s18 (2007).
57. Hoff, K. J., Lange, S., Lomsadze, A., Borodovsky, M. & Stanke, M. BRAKER1: Unsupervised RNA-Seq-Based Genome Annotation with GeneMark-ET and AUGUSTUS. *Bioinformatics* **32**, 767-769 (2016).
58. Kim, D. *et al.* TopHat2: accurate alignment of transcriptomes in the presence of insertions, deletions and gene fusions. *Genome Biol* **14**, R36, doi:10.1186/gb-2013-14-4-r36 (2013).
59. Li, H. *et al.* The Sequence Alignment/Map format and SAMtools. *Bioinformatics* **25**, 2078-2079 (2009).
60. Lomsadze, A., Burns, P. D. & Borodovsky, M. Integration of mapped RNA-Seq reads into automatic training of eukaryotic gene finding algorithm. *Nucleic Acids Res* **42**, e119, doi:10.1093/nar/gku557 (2014).
61. Stanke, M., Diekhans, M., Baertsch, R. & Haussler, D. Using native and syntenically mapped cDNA alignments to improve de novo gene finding. *Bioinformatics* **24**, 637-644 (2008).
62. Wang, X. *et al.* The locust genome provides insight into swarm formation and long-distance flight. *Nat Commun* **5**, 2957, doi:10.1038/ncomms3957 (2014).
63. The International Aphid Genomics Consortium. Genome sequence of the pea aphid *Acyrthosiphon pisum*. *PLoS Biol* **8**, e1000313, doi:10.1371/journal.pbio.1000313 (2010).
64. Gramates, L. S. *et al.* FlyBase at 25: looking to the future. *Nucleic Acids Res* **45**, D663-D671, doi:10.1093/nar/gkw1016 (2017).
65. McKenna, D. D. *et al.* Genome of the Asian longhorned beetle (*Anoplophora glabripennis*), a globally significant invasive species, reveals key functional and evolutionary innovations at the beetle-plant interface. *Genome Biol* **17**, 227, doi:10.1186/s13059-016-1088-8 (2016).
66. Xue, J. *et al.* Genomes of the rice pest brown planthopper and its endosymbionts reveal complex complementary contributions for host adaptation. *Genome Biol* **15**, 521, doi:10.1186/s13059-014-0521-0 (2014).

67. Benoit, J. B. *et al.* Unique features of a global human ectoparasite identified through sequencing of the bed bug genome. *Nat Commun* **7**, 10165, doi:10.1038/ncomms10165 (2016).
68. Suyama, M., Torrents, D. & Bork, P. BLAST2GENE: a comprehensive conversion of BLAST output into independent genes and gene fragments. *Bioinformatics* **20**, 1968-1970 (2004).
69. Birney, E., Clamp, M. & Durbin, R. GeneWise and Genomewise. *Genome Res* **14**, 988-995 (2004).
70. Grabherr, M. G. *et al.* Full-length transcriptome assembly from RNA-Seq data without a reference genome. *Nat Biotechnol* **29**, 644-652 (2011).
71. Xu, Y., Wang, X., Yang, J., Vaynberg, J. & Qin, J. PASA--a program for automated protein NMR backbone signal assignment by pattern-filtering approach. *J Biomol NMR* **34**, 41-56 (2006).
72. Haas, B. J. *et al.* Automated eukaryotic gene structure annotation using EVidenceModeler and the Program to Assemble Spliced Alignments. *Genome Biol* **9**, R7, doi:10.1186/gb-2008-9-1-r7 (2008).
73. Yang, Y. *et al.* Draft genome of the Marco Polo Sheep (*Ovis ammon polii*). *GigaScience* **6**, 1-7, doi:10.1093/gigascience/gix106 (2017).
74. Finn, R. D. *et al.* InterPro in 2017-beyond protein family and domain annotations. *Nucleic Acids Res* **45**, D190-D199, doi:10.1093/nar/gkw1107 (2017).
75. Bairoch, A. & Apweiler, R. The SWISS-PROT protein sequence database and its supplement TrEMBL in 2000. *Nucleic Acids Res* **28**, 45-48 (2000).
76. Jones, P. *et al.* InterProScan 5: genome-scale protein function classification. *Bioinformatics* **30**, 1236-1240 (2014).
77. The Gene Ontology Consortium. Expansion of the Gene Ontology knowledgebase and resources. *Nucleic Acids Res* **45**, D331-D338, doi:10.1093/nar/gkw1108 (2017).
78. Adams, M. D. *et al.* The genome sequence of *Drosophila melanogaster*. *Science* **287**, 2185-2195 (2000).
79. Gotz, S. *et al.* High-throughput functional annotation and data mining with the Blast2GO suite. *Nucleic Acids Res* **36**, 3420-3435 (2008).
80. Kanehisa, M., Sato, Y. & Morishima, K. BlastKOALA and GhostKOALA: KEGG tools for functional characterization of genome and metagenome sequences. *J Mol Biol* **428**, 726-731 (2016).
81. Tang, H. *et al.* ALLMAPS: robust scaffold ordering based on multiple maps. *Genome Biol* **16**, 3, doi:10.1186/s13059-014-0573-1 (2015).
82. Kent, W. J. *et al.* The human genome browser at UCSC. *Genome Res* **12**, 996-1006 (2002).
83. Pascoal, S. *et al.* Sexual selection and population divergence I: The influence of socially flexible cuticular hydrocarbon expression in male field crickets (*Teleogryllus oceanicus*). *Evolution* **70**, 82-97 (2016).
84. Catchen, J., Hohenlohe, P. A., Bassham, S., Amores, A. & Cresko, W. A. Stacks: an analysis tool set for population genomics. *Mol Ecol* **22**, 3124-3140 (2013).
85. Li, H. & Durbin, R. Fast and accurate short read alignment with Burrows-Wheeler transform. *Bioinformatics* **25**, 1754-1760 (2009).
86. Calus, M. P. Genomic breeding value prediction: methods and procedures. *Animal* **4**, 157-164 (2010).
87. VanRaden, P. M. Efficient methods to compute genomic predictions. *J Dairy Sci* **91**, 4414-4423 (2008).
88. Donoughe, S. & Extavour, C. G. Embryonic development of the cricket *Gryllus bimaculatus*. *Dev Biol* **411**, 140-156 (2016).
89. Joshi, N. A. & Fass, J. N. *SICKLE: a sliding-window, adaptive, quality-based trimming tool for FastQ files [Software]*, <https://github.com/najoshi/sickle> (2011).
90. Pertea, M., Kim, D., Pertea, G. M., Leek, J. T. & Salzberg, S. L. Transcript-level expression analysis of RNA-seq experiments with HISAT, StringTie and Ballgown. *Nat Protoc* **11**, 1650- 1667 (2016).
91. Robinson, M. D., McCarthy, D. J. & Smyth, G. K. edgeR: a Bioconductor package for differential expression analysis of digital gene expression data. *Bioinformatics* **26**, 139-140 (2010).
92. Kanehisa, M., Sato, Y., Kawashima, M., Furumichi, M. & Tanabe, M. KEGG as a reference resource for gene and protein annotation. *Nucleic Acids Res* **44**, D457-462, doi:10.1093/ nar/gkv1070 (2016).
93. Schneider, W. T., Rutz, C., Hedwig, B. & Bailey, N. W. Vestigial singing behaviour persists after the evolutionary loss of song in crickets. *Biol Lett* **14**, doi:10.1098/rsbl.2017.0654 (2018).
94. Li, S. *et al.* The genomic and functional landscapes of developmental plasticity in the American cockroach. *Nat Commun* **9**, 1008, doi:10.1038/s41467-018-03281-1 (2018).
95. Rosenfeld, J. A. *et al.* Genome assembly and geospatial phylogenomics of the bed bug *Cimex lectularius*. *Nat Commun* **7**, 10164, doi:10.1038/ncomms10164 (2016).
96. Terrapon, N. *et al.* Molecular traces of alternative social organization in a termite genome. *Nat*

Commun **5**, 3636, doi:10.1038/ncomms4636 (2014).

97. Dudchenko, O. *et al.* De novo assembly of the *Aedes aegypti* genome using Hi-C yields chromosome-length scaffolds. *Science* **356**, 92-95 (2017).
98. Miller, J. R. *et al.* Analysis of the *Aedes albopictus* C6/36 genome provides insight into cell line utility for viral propagation. *GigaScience* **7**, 1-13, doi:10.1093/gigascience/gix135 (2018).
99. Majlat, P., Erdos, Z. & Takacs, J. Calculation and application of retention indexes in programmed-temperature gas-chromatography. *J Chromatogr* **91**, 89-103 (1974).